Master Thesis

Fabrication of bioactive macro-size scaffolds using multiphoton polymerization for Tissue Engineering Applications

carried out for the purpose of obtaining the degree of Master of Science (MSc or Dipl.-Ing. or DI), submitted at TU Wien, Faculty of Mechanical and Industrial Engineering, by

Theresia Baumgartner

Mat.Nr.: 01225892

under the supervision of
Univ. Prof. Dr.rer.nat Aleksandr Ovsianikov
and Univ. Ass. Dr. Olivier Guillaume
Institute of Materials Science and Technology,
Research Group for 3D Printing and Biofabrication

Vienna, June 2021

This work was supported by the European Research Council (ERC) within the framework of the Consolidator Grant project Third Strategy in Tissue Engineering – Functional microfabricated multicellular spheroid carriers for tissue engineering and regeneration (THIRST)

I confirm, that going to press of this thesis needs the confirmation of the examination committee.

Affidavit

I declare in lieu of oath, that I wrote this thesis and performed the associated research myself, using only literature cited in this volume. If text passages from sources are used literally, they are marked as such.

I confirm that this work is original and has not been submitted elsewhere for any examination, nor is it currently under consideration for a thesis elsewhere.

I acknowledge that the submitted work will be checked electronically-technically using suitable and state-of-the-art means (plagiarism detection software). On the one hand, this ensures that the submitted work was prepared according to the high-quality standards within the applicable rules to ensure good scientific practice "Code of Conduct" at the TU Wien. On the other hand, a comparison with other student theses avoids violations of my personal copyright.

_____   _____
City and Date   *Signature*

Abstract

Two-Photon polymerization (2PP) is a promising additive manufacturing method, which enables the fabrication of complex three-dimensional objects using computer aided design (CAD). It relies on the interaction of femtosecond laser pulses with special photosensitive materials. The main advantage of 2PP compared to other additive manufacturing techniques is that resolutions in the sub-micron range can be achieved. The downside however is the increase in fabrication time, especially for larger structures. A growing field of interest is the use of 2PP for the fabrication of macro-sized scaffolds for different tissue engineering approaches since this technology is capable of reproducing the microstructure of different tissue types.

The aim of this thesis was to design, print and develop strategies to functionalize a stable and bioactive macro scaffold via 2PP by using a novel material called hexa-acrylate end-capped urethane-based poly- ε-caprolactone (UPCL-6). The initial fabrication strategy was further optimized resulting in a high-quality macro-scaffold. The as obtained material was subsequently functionalized to endow the printed scaffolds with bioactive properties. The surface was initially functionalized with amine groups allowing for an increased uptake of heparin onto its surface. The heparin in turn was able to efficiently bind to several growth factors used in this study. In a second step, the fibroblast growth factor (FGF-2), was indirectly bound onto the surface modified with heparin. The bioactivity of FGF-2 was analyzed using enzyme-linked immunosorbent assay (ELISA).

In this thesis a macro-size scaffolds with a diameter of up to 6000 μm were fabricated via 2PP. This was realized by improving the work protocol of the material preparation. The structure was further optimized by improving the porous structure design.

The biofunctionalization process to modify the surface of the structure was enabled by covalently binding heparin on the aminolysed surface.

Kurzfassung

Zwei-Photonen Polymerisation (2PP) ist eine vielversprechende additive Fertigungsmethode, die es ermöglicht, komplexe Strukturen zu erstellen. Um die gewünschten Ergebnisse zu erreichen, müssen die Strukturparameter an das angewendete Material und Design angepasst werden. Der wichtigste Vorteil von 2PP im Vergleich zu anderen additiven Fertigungstechniken ist, dass Auflösungen im Submikrometerbereich erreicht werden können. Der Nachteil von 2PP ist jedoch die längere Herstellungszeit, insbesondere bei größeren Strukturen. Ein wachsendes Interessengebiet für 2PP ist „Tissue Engineering", da durch die Herstellung komplexer Strukturen und den Einsatz neuer Materialien kommt es vermehrt in der Entwicklung biomedizinischer Anwendungen zum Einsatz.

Das Ziel dieser Arbeit war es, eine stabile und bioaktive makrogroße Struktur mittels 2PP zu entwerfen, zu drucken und zu entwickeln. Dabei wurde ein neuartiges Material namens hexaacrylate end-capped urethanbasiertes Poly-ε-Caprolacton (UPCL-6) verwendet. Die anfängliche Herstellungsstrategie wurde weiter optimiert, dass zu einer hochwertigeren Struktur führte. Darüber hinaus wurden Strategien der Funktionalisierung entwickelt, um gedruckte Strukturen mit bioaktiven Eigenschaften auf deren Oberflächenumgebung auszustatten. Im ersten Schritt wurde das Material aminolysiert, um im nächsten Schritt eine höhere Menge an Heparin kovalent an die Oberfläche zu binden. Heparin ist dafür bekannt, eine hohe Bindungseffizienz an verschiedene Wachstumsfaktoren zu haben. In einem zweiten Schritt wurde der Wachstumsfaktor namens FGF-2 verwendet und indirekt an die modifizierte Oberfläche gebunden. Die Bioaktivität des Wachstumsfaktors wurde mittels Enzyme-Linked Immunosorbent Assay (ELISA) analysiert.

In dieser Arbeit wurde eine Struktur mit einem Durchmesser von 6000 μm mittels 2 PP hergestellt. Dies wurde durch das verbesserte Protokoll für die Materialvorbereitung erreicht und durch das optimierte Design konnte eine höhere Qualität erreicht. Die Biofunktionalisierung zur Modifizierung der Oberfläche wurde durch die kovalente Bindung von Heparin an die bereits aminolysierte Oberfläche ermöglicht werden. Die Bindung von FGF-2 mit einer sensibleren Methode untersucht werde.

Acknowledgements

I would like to use this opportunity to thank all people, who supported me during my studies and especially during this thesis.

First of all, I would like to thank my supervisors Aleksandr Ovsianikov and Olivier Guillaume for supporting me throughout my studies and allowing me to work in this fascinating science field.

My special thanks go to my colleagues at the Research Group for 3D Printing and Biofabrication. It was my pleasure to work with them, ask questions and get help when I needed it.

I would particularly like to express my thanks to Marica Markovic for her help in the lab, for being there for me and always encouraging me to persist and finish my thesis. Furthermore, I want to thank Oliver Kopinski-Grünwald for helping me choose the right design and Franziska Gantner for assisting me to resolve numerous problems and challenges.

I also want to thank my friends, who were there for me when I needed them. A special thanks to Katharina, with whom I spent countless hours studying and working together.

Lastly, I want to express my gratitude to my family and especially my parents for their unconditional support.

Most of all, I want to thank my partner Maximilian who has always encouraged me to persevere and believed in me, supporting my studies from the beginning to the end.

Table of Contents

1 Introduction

Osteochondral defects are a joint damage that occur in certain body areas when the articular cartilage and the adjacent subchondral bone are damaged.[1] This can result in a substantial reduction of the quality of life because it can cause pain, swelling, limitation in physical function and activity.[2] A review of 25 124 arthroscopies showed that the osteochondral defect is highly common. In total, 67% of the documented cartilage lesions were classified as an osteochondral or chondral lesions, frequently in the medial formal condyle – medial to the knee.[3] Osteochondral defects can also accelerate the progress of degenerative diseases such as osteoarthritis.[4] In 2016 World Health Organization has published that 240 million people over the world suffer from osteoarthritis and the estimation shows that about 9.6% of men and 18.0% of women older than 60 years have symptomatic osteoarthritis. It is expected that this number will increase over the next years because of an increasing number of patients with obesity and high body mass index which are risk factors for osteoarthritis development.[5, 6]

There are several options for cartilage treatment which can be classified in two main groups: conservative or surgical treatment.[7] Conservative treatment has a wide spectrum of methods including weight loss to reduce the load on knee joints, physical exercises, or the use of non-steroid anti-inflammatory drugs, pain killers or hormones. The alternative surgical treatment is still a major challenge in the orthopedic field and the operability depends on the lesion size, cause, age, activity level and severity, and depth of the osteochondral defect.[7] A total replacement of the knee is only performed on patients of a certain age and if the damage to the tissue is too severe. However, it is still an effective treatment for progressed osteoarthritis cases.[7]

The main challenge for optimal treatment of osteochondral defects is to regenerate the damaged tissue.[1, 4, 8] This problem is addressed by tissue engineering and regenerative medicine (TERM) which offers promising new approaches for osteochondral tissue regeneration. The main idea of this emerging field is the replacement or regeneration of parts of the human body, for example tissue or cells. For this process to work several key components have to be taken into account which can be classified as biological factors (such as cell types and growth factors), properties of the scaffold material (for example mechanical behavior), and the fabrication methods.[9]

Scaffolds, which can be understood as a three-dimensional (3D) porous structure in which cells are grown, play a significant part in TERM.

The porous scaffolds should support the cell growth and thereby the regeneration of tissue, [4]

but the mechanical structure is undoubtedly not the only function of a scaffold. A key requirement is that the material of the scaffold has to be both biocompatible and biodegradable. Consequently, as the choice of materials is quite limited, traditional fabrication methods are typically not suitable due to the highly complex required 3-dimensional shape required. However, additive manufacturing can be used as it allows for the fabrication of (arbitrary) 3D objects. Especially two-photon polymerization (2PP) is a highly promising method since it enables the fabrication of scaffolds with a sub-micrometer spatial resolution.

The main advantage of 2PP compared to the very similar stereolithography (SLA) is that feature sizes in the order of 100 nm can be achieved. The major concern however is that the fabrication of large scaffolds is time-consuming and the necessary stitching of adjacent fields of view (FOV) will leave noticeable transitions in the material. The dimension of one FOV is approximately 800 µm and the sample stage of the 2PP system has to move and position the sample in a way that a second adjacent FOV can be printed. Furthermore, the application in tissue engineering is limited by the availability of biocompatible and biodegradable photopolymers and suitable photoinitiators. The first scaffold of macroscopic size fabricated by 2PP was reported by Weisgrab *et al* 2020 with a size of 18 x 18 x 0.9 mm (equaling 292 mm³).[10]

As most of the synthetic scaffolds have a lack of bioactivity it is necessary to introduce growth factors (GF) on the surface of the applied material. GFs like fibroblast GF are soluble signaling proteins that have been used in tissue engineering to promote cell differentiation.[11]

The aim of this thesis was the fabrication of a printable macro-size scaffold using 2PP and the biofunctionalization of the surface. Therefore, it was necessary to develop a suitable design and to improve the UPCL-6 material preparation. Subsequently heparin was covalently bound to priorly introduced amino groups of the surface of UPCL-6. The growth factors were bound indirectly to the heparin to achieve a bioactive macro-size scaffold.

2 Theoretical Background

2.1 Additive manufacturing

Additive manufacturing (AM) is technology based on the fabrication of 3D objects by addition of material instead of subtraction from a raw part.[12] In the last two decades, this technology is especially dominant in the prototype market and in small-scale production. An advantage is the ability to design complex structures which are typically not accessible via traditional subtractive methods, as well as allowing for rapid prototyping of parts. However, the complexity of the process makes it expensive and time-consuming. The methods subsumed under the term AM range from simply fused layer deposition (FLD) or laser sintering to more complex processes like stereolithography (SLA) or multi-photon absorption (MPA), which includes the 2PP process. [12] SLA as well as MPA are so-called resin 3D printing techniques, which other than FLD, rely on the local polymerization of a photosensitive resin and thus ensue in higher printing quality. However, some of its drawbacks are an increased printing time, and typically more expensive materials. In comparison with MPA, SLA is a based on 1-photon absorption. The advantages of this method are that the high degree of porosity and any design can be achieved. However, the resolution is limited to around 20 µm.[13] MPA-processes, which are based on multi-photon absorption, more specifically on two-photon absorption (2PA) that allow for a feature size down to a few 100 nm. This high local resolution is achieved by 2PA which will be discussed in detail in the following sections.

2.1.1 Multi-photon absorption

In 1931 Maria Göppert-Mayer published the first theoretical article describing the phenomena of multi-photon absorption (MPA). It describes the excitation of an atom in a higher energy state by simultaneous absorption of two or more photons.[14] The easiest problem for multi-photon absorption (MPA) is the so-called two-photon absorption (2PA). Absorption of photons is a resonance process thus only photons with an energy equal to the energy separation between two states can excite a molecule. In the case of 2PA one photon alone would not have sufficient energy to excite the molecule, however, if 2 photons of, typically, the same energy are absorbed at virtually the same time (due to energy-time-uncertainty the timeframe is in the range of 0.1 fs) the molecule can be excited if the sum of the two-photon energies is the same as the energy difference between the ground and the excited state. In this case, a higher energy state is reached by the simultaneous absorption of 2 photons of the appropriate energy whereas each of the

single photons would not be able to excite the molecule (see Figure 1 on the right).[15] The short time frame, however, makes this process very improbable, thus a high local and temporal photon density has to be achieved to observe it. Only with the invention of the laser those requirements were met allowing Kaiser and Garrett to experimentally validate the theory of 2PA.[16]

In general, the absorption of light can initiate physical or chemical reactions. In the linear case the absorption takes place along the entire light path as described by Beer-Lambert law (see Figure 1 on the left). For 2PA on the other hand, absorption can only take place in a spatially very focused region due to the non-linearity of the process. As a consequence, excitations will only occur in the focus point.[17] This can be used, for example, in 2-photon microscopy where molecules are activated locally and then lose their energy through fluorescence – the emission of a photon- allowing for high-resolution images of thick tissue samples.[18].
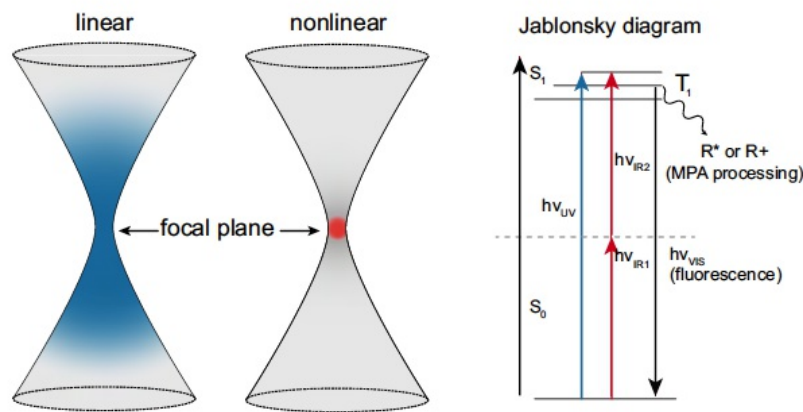

Figure 1: Illustration of linear and nonlinear absorption principle (left) and Jablonsky diagram (right) linear and 2-photon cases [19]

2.1.2 Multi-photon lithography system

A schematic representation of the multi-photon lithography setup used during the present work is shown in Figure 2. The device was developed by Gruber.[19] The laser beam is produced by a tunable, pulsed high-power femtosecond Ti:Sapphire laser (MaiTai eHP DeepSe, Spectra-Physics). The wavelength can be adjusted between 690 nm and 1040 nm. The pulse width is 70 fs, the average power 2.4 W and the repetition rate 80 MHz. The linearly polarized beam is passed through a rotating achromatic wave plate followed by a polarizing beam splitter cube which transmits the p-polarized part of the light and reflects the s-polarized part into a beam dump, thereby allowing an adjustment of the system. Subsequently, an acousto-optic-modulator

(AOM, AA Opto-Electronic) is used to achieve a fast power modulation of the laser beam before it is transmitted through a pinhole ensuring that only the first order laser beam is used. Furthermore, the AOM is used as a shutter. The use of a 5x achromatic beam expander makes sure that the beam expands to the back aperture of the objective to obtain a small, focused laser beam. A galvanometer-scanner (Scanlab) detects the position of the laser beam and allows for its precise control in the x and y-direction. The laser beam is then passed through a tube lens and a microscope objective, which focuses the laser beam onto the stage.

The stage allows the movement of the sample in XY-direction while the objective controls the position of the focal point in z-direction. A complementary metal-oxide semiconductor (CMOS) camera positioned along the optical axis allows for the observation of the printing process in real-time.[19]
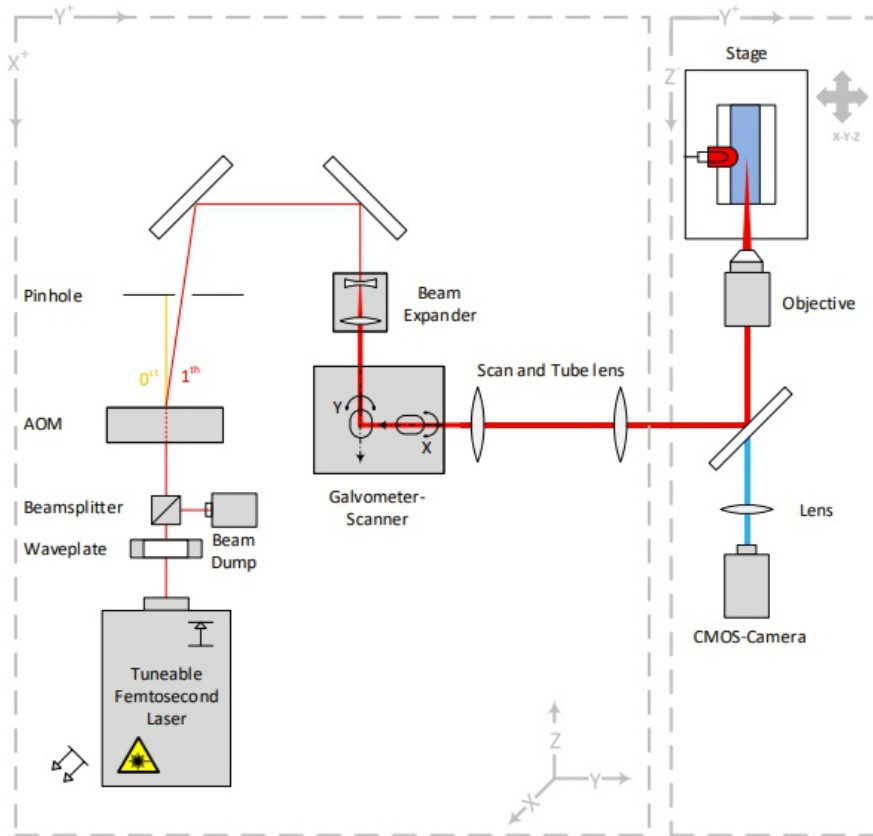

Figure 2: schematic illustration of the used 2PP system in the present work [19]

2.1.3 Field of view

During the printing process only a small area (approx. 800 µm), called field of view (FOV), is accessible by laser scanning. To obtain a structure large than the FOV the sample is moved allowing the laser to illuminate a new area. The difficulty lies in the joining of the neighboring FOVs, and the process is typically called stitching. If the two regions do not overlap two separate parts will be formed however if the parts overlap to much a joint will be visible. Furthermore, if the part is misplaced or rotated slightly misalignments of FOVs can be the consequence. These imperfections can result in unwanted gaps in the final parts.[10, 20, 21]

2.1.4 Polymerization

Polymerization is a general term describing a chemical process in which small molecules, also called monomers in this context, react to form large molecules, called polymers, which consist of repeating monomer units. Polymerization reactions are classified into either [22]:

- condensation and addition reactions based on the composition or structure of the polymer, or
- step and chain reactions that are depended on the mechanisms of the polymerization process.

The difference between a condensation polymerization and an addition reaction is that during condensation small molecules such as water are eliminated. An example is a polyester, which is formed by the reaction of diacids with diols under the elimination of water. Addition polymerization on the other hand forms polymers without the formation of side products.[22]

The second classification is based on the mechanism of the reaction taking place during the polymer formation, separating step and chain polymerization.

Step polymerization proceeds by stepwise intermolecular reaction between functional groups of the monomers. The first step is that two monomers react with each other forming a dimer. The dimer subsequently reacts with an additional monomer forming a trimer and so on. The polymerization continues stepwise and when approaching the end, the polymerization rate is increasing rapidly.[23]

Other than in a step polymerization for a chain polymerization taking place, an initial reactive center, such as a free radical, cation or anion, has to be formed by the addition of an initiator.

Subsequently, the monomer units only react with the reactive center. Polymerization occurs by the propagation of the reactive center through successive additions of large numbers of monomer molecules in a chain reaction. In 2PP most materials follow a chain polymerization. The mechanism of the chain reaction can be separated into three elementary steps: initiation, propagation and termination.[22] In the first step, an initiator molecule is decomposed forming 2 radical species. The radical species then react with a double bond of a monomer forming a primary radical.[23] In the second step, the primary radical reacts with other monomers in multiple steps until no monomer is left or termination occurs.[24] At the termination step, the polymerization ends by eliminating the active center either by recombination of two radicals or by disproportionation.[23]

2.1.5 Two-Photon polymerization

As discussed above, the initial step of a radical polymerization is the formation of 2 radicals from an initiator molecule. This can be achieved, for example thermally, or in the case of radical photopolymerization by using a so-called photo-initiator (PI) which forms radicals under the irradiation with light of the appropriate energy.

Due to the PI, polymerization can be confined to specific regions. There are two ways that light absorption results in the formation of radicals: [22]

1) PI molecules in the system are excited by energy absorption and subsequently decompose into radicals, or

2) a combination of molecules is used as PI where one molecule is excited and then interacts with a second compound by either energy transfer or a redox reaction.

The main advantage of photopolymerization is that it is faster and more energy efficient than a thermally activated polymerization. Furthermore it allows for the reaction to be triggered in a very confined region.[24] For 2PP commercially available PIs have been used initially but the achievable writing speed is slow, high laser power is required and the resolution of the structure is compromised. This is caused due to their low efficiency for two-photon absorption. Therefore, specially designed PIs were developed such as 4-methylcyclohexanone-based initiator (M2CMK).[24]

2.1.6 UPCL-6 for scaffold fabrication

As discussed above commercially available resins often lack the requirements for tissue engineering, especially the biocompatibility and -degradability thus polymers are developed with this application in mind. The material used in this work is so-called hexaacrylate end-capped urethane-based poly- ε-caprolactone (UPCL-6) which was specially developed to use the true capabilities of 2PP for TE applications.[25] The well-known precursor poly- ε-caprolactone (PCL) diol, a hydrophobic, semi-crystalline polymer, has been modified via a 2 step-synthesis (Figure 3). First, the PCL-diol has reacted with isophorone diisocyanate (IPDI) and in the second step ethoxylated and propoxylated pentaerythritol triacrylate was added as an agent for end-capping. The molar mass for the resin UPCL-6 is 11 300 g mol^{-1}.[25] UPCL-6 was especially synthesized for the use in 2PP with the aim to improve mechanical strength and processability.
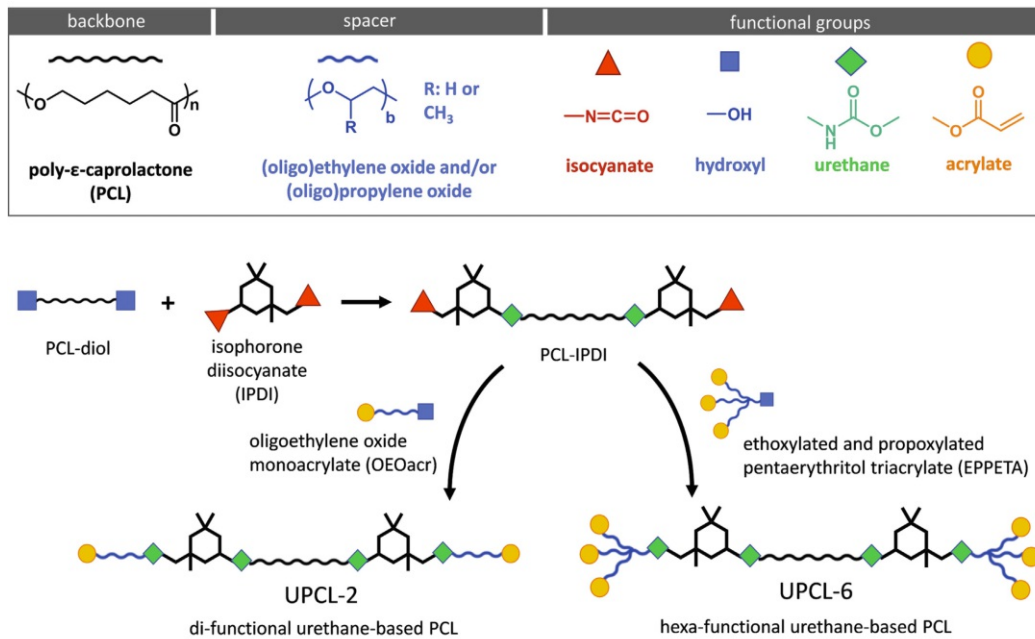
Figure 3: mechanism of developing UPCL-6 [25]

2.2 Tissue Engineering

In 1988 at a National Science Foundation workshop, the term Tissue Engineering (TE) was officially introduced subsuming "the application of principles and methods of engineering and life sciences toward the fundamental understanding of structure-function relationships in normal and pathological mammalian tissues and the development of biological substitutes to restore, maintain or improve tissue function".[26]

In the last decades, different technological approaches of TE were developed with the aim to restore, replace or regenerate defective tissues. The methods can be classified into scaffold-based and scaffold-free strategies.[27]

The idea of using a scaffold is to create a temporary structure supporting the initial cell attachment, proliferation, and formation of new extracellular matrix.[28] A scaffold can be a 3D porous structure, a hydrogel where cells are embedded or a combination of both.[29]

Scaffolds have to comply with certain properties to be used in TE. First, the material of the scaffold has to be biocompatible, biodegradable, and the mechanical, as well as surface chemical properties, have to be appropriate for cell attachment, proliferation and differentiation. The scaffold should furthermore be comprised of an interconnected porous structure.[26, 28]

The strategy of scaffold-free TE on the other hand is based on tissue spheroids and the idea of self-assembly. This approach is a special case in 3D cell culture, where multiple cells are fused to create a 3D spheroid.[30, 31]

3 Materials and Methods

3.1 Photoinitiator

In this study, two different photoinitiators (PI) were used: 2,4,6-trimethylbenzoyl phenylethoxyphospine oxide (TPO-L) and a 4-methylcyclohexanone-based initiator (M2CMK).

TPO-L is a commercially available (SpeedCure, Lambson) one photon absorption PI which absorbs ultraviolet A and blue light. TPO-L is a liquid that can be mixed with material formulation.[24] The structure of TPO-L is presented in Figure 4.
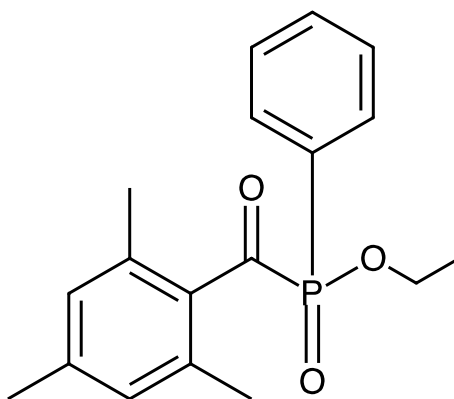
Figure 4: Molecular structure of TPO-L

M2CMK is a highly active two-photon absorption photoinitiator synthesized via a classical aldol condensation reaction. It is an organo-soluble initiator and well suited for high writing speeds in the 2PP manufacturing process[32]. M2CMK was synthesized and provided by the Research Group for Polymer Chemistry and Technology, TU Wien. The structure of M2CMK is presented in Figure 5.
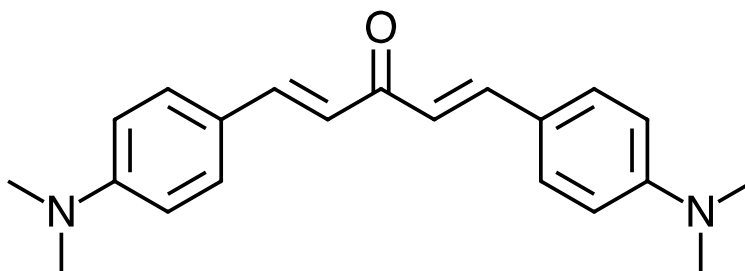
Figure 5: Molecular structure of M2CMK

3.2 UPCL-6 coating of glass coverslips

The biofunctionalization of UCPL-6 was first optimized on films (2D) before performing it on 3D scaffolds. Initially, the glass coverslip surface used for the 2D experiments was functionalized with methacrylate groups to allow for the adhesion of UPCL-6 to the glass surface.

The methacrylation of coverslips was carried out following the protocol:

For salinization, 18 mm cover glasses (Carl Roth) loaded in appropriate staining racks were pre-treated in a plasma cleaner (Harrick Plasma) for 10 min to remove all organic matter from the surface. Afterwards they were soaked in a methacrylate solution consisting of deionized water (50% v/v), ethanol (48% v/v), glacial acetic acid (0.3% v/v) and 3-(trimethoxysilyl)-propyl methacrylate (2% v/v). After a contact time of 30 min, the liquid was removed and the now coated glasses were rinsed twice with deionized water. In the last step, the cover glasses were dried in an oven for 30 min at 110°C.

After methacrylation of coverslips, coating with UPCL-6 was performed

- UPCL-6 (85 mg) was dissolved in 700 µL tetrahydrofuran (THF, Sigma) for several minutes to prepare the material required for 10 coverslips.

- 20 µL of TPO-L (3.6 mM TPO-L) were added to the UPCL-6.

- 70 µL of the prepared mixture were pipetted in the middle of each methacrylated coverslip and heated at 50 °C for 3 hours.

- To cross-link the polymer, the coated glasses were exposed to UV light ($\lambda = 365$ nm) for 5 min with 1 J.

- The obtained coated glasses were used for testing biofunctionalization.

3.3 UPCL-6 material preparation

The preparation of UPCL-6 for printing was performed in two different manners to optimize the working protocol.

A stock solution of 10 mM M2CMK was prepared in a 5 mL tinted glass vial to prevent PI exposure to ambient light. For this the appropriate volume of THF was calculated according to equation (1):

$$THF\ [mL\ ] = \frac{PI\ [g]}{374.52\left[\frac{g}{mol}\right]*0.00001\left[\frac{mol}{mL}\right]} \tag{1}$$

where PI stands for the weight in of the M2CMK, 374.52 is the molecular weight of M2CMK in g/mol, 0.00001 is correction factor for converting mM to M and mL to L.

UPCL-6 (approximately 1g) was weighed into a 5 mL tinted glass to prevent material exposure to the light. UPCL-6 was dissolved by using the 10 mM M2CMK stock solution. The required volume can be calculated as shown in Equation 2:

$$PI\ Stock\ solution\ [mL] = \frac{0.005*m_{UPCL-6}\ [g]}{374.52\left[\frac{g}{mol}\right]*0.00001\left[\frac{mol}{mL}\right]} \tag{2}$$

where m_{UPCL-6} stands for the weight in of the UPCL-6 resin, 374.52 is the molecular weight of M2CMK in g/mol, 0.00001 is correction factor for correction factor for converting mM to M and mL to L, 0.005 is factor for 0.5 wt % of M2CMK, final concentration of PI in the resin.

To prepare the coverslips 18x18 mm (Carl Roth, Germany) for the attachment of the resin they were glued onto a custom-made metal sample holder with three quadratic cut-outs of the size of the glass using two-component dental glue. In Figure 6, a picture of the sample holder where the cut-outs with the coverslips are already filled with resin is shown.

The coverslips were then covered with resin and treated with varying parameters (heating temperature, evaporation times and amount of resin per sample holder) to optimize the samples.

An overview of varied parameters is presented in Table 2 in results section 4.1.2 and will be discussed in detail there.

Two different procedures were used for the preparation of the samples. Initially, method 1 was used, however due to difficulties with the retention of THF in the resin, which in turn led to problems especially during the printing stage.

1. Layer by layer deposition:

500 µL of the dissolved resin was pipetted into the sample holder as a thin layer, the sample holder was placed on a heat block at 70 °C for 1 h to evaporate THF. After 1 h, THF should be completely evaporated, and a second layer was pipetted onto the first one and again the resin was heated for 1 h. These steps were repeated until a total layer height of 1.5 mm was reached (2-3 layers). The resin was pre-heated on a heat block to 50 °C for 10 min before printing to ensure that the material stays transparent.

2. Bulk deposition:

Other than with method 1 the whole amount of prepared resin required to fill the cavity was pipetted in at once. Subsequently the samples were placed on a heat block at 120 °C for 2-3 h, until no more air bubbles were visible in the sample. Before printing the resin was pre-heated to 50 °C for 10 min to ensure material transparency.

Figure 6: sample holder with 2 cutouts filled with the UPCL-6 resin

3.3.1 Sample development

After printing the obtained structured samples were submerged in THF overnight detaching them from the glass plate and sample holder, and furthermore removing any unpolymerized resin. On the next day, the THF solution was exchanged with fresh THF, and the printed scaffold was washed twice for 30 minutes. After the last washing step, hexamethyldisilazane (HMDS, Sigma Aldrich) was carefully pipetted on the scaffold completely covering the sample surface and subsequently dried in a laminar flow hood. The aim of using HMDS is to reduce the surface tension and prevent defects from occurring during the drying process.

3.3.2 Printing process

The designs of the scaffolds were created using Inventor Professional (Autodesk Inc., USA), which is a common software for 3D-computer aided design (CAD). The format of the files was standard transformation language (stl.). The 2PP printing setup used for this work has been built previously in our laboratory, and it has been described in chapter 2.1.2.[19]

For all performed experiments during fabrication steps, an Olympus 10x/0.4 NA objective (UPlanSApo, 10x/0.4 NA, Olympus, Japan) was used. The printing was performed in the top to bottom mode, to prevent the laser from irradiating already photopolymerized regions. The power of the laser beam after the microscope objective was set to a value of 85 mW. Furthermore, the laser operated at a wavelength of 800 nm and at a pulse duration of 70 fs. The writing speed was set to 1 000 mm/s.

The fabrication time of a macro-size scaffold was minimized by using 1.5 μm for the line spacing (also called hatch) and layer spacing for the inner part of the scaffold and 5 μm for the ring-shaped frame. In Table 1 an overview of the parameters used is given.

Table 1: Used parameters for printing to fabricate a scaffold

Laser wavelength [nm]	800	
Laser intensity [mW]	85	
Block height [μm]	150	
Stitching overlap [μm]	10	
Writing speed [mm/s]	1000	
Stitching half angle [°]	14	
Line spacing (hatch) [μm]	1.5	
Layer spacing (dz) [μm]	1.5 (scaffold)	5 (frame)

3.4 Biofunctionalization of macro-size scaffolds

As discussed above, a key point of the scaffolds for tissue engineering is their biocompatibility. Thus, the samples used in this study were first modified with an aminolysis reaction that allowed the immobilization of heparin. In the last step, indirect binding of growth factors was attempted. Initially, water and ethanol were used as a solvent for the first two steps. However, due to the high surface-to-volume ratio, the 3D-printed-micro-size scaffolds did tend to stick to each other and could not be separated anymore. This could be circumvented by changing the solvent to 1-propanol.

The strategies were first evaluated and optimized on 2D UPCL-6 coated coverslips and afterwards applied to the 3D scaffolds.

3.4.1 Surface modification of UPCL-6 surface via aminolysis

First, amino groups were covalently introduced onto UPCL-6 surface by the reaction between ester groups of UPCL-6 and 1,6-Hexanediamine. The reaction schematic is presented in Figure 7.
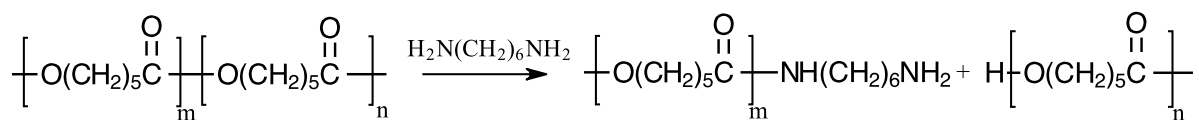
Figure 7: schematic presentation of aminolysis of PCL-6 molecular with 1,6-hexandeamine

The protocol for surface modification of polycaprolactone membrane via aminolysis and biomacromolecule immobilization [33] was adapted to introduce amino groups and following steps were carried out:

- First UPCL-6 scaffolds were immersed in 1-propanol for 2-3 h to clean the surface and afterwards, it was thoroughly washed with 1-propanol.

- The now cleaned scaffolds were immersed in 0.43 mol/L 1,6-hexanediamine/1-propanol solution for 1 h at 30 °C and washed with copious amounts of 1-propanol. To ensure the complete removal of remaining reactant they were submerged in 1-propanol overnight.

To prove the success of aminolysis a ninhydrin assay [34] was carried out. The UPCL-6 sample was immersed in 1 mol/L ninhydrin/ethanol solution and the reaction was accelerated by

incubation at 80 °C for 15min. The ninhydrin will react with the amino groups forming a deep purple diketohydrin, also known as Ruhemann's purple which then allowed for a qualitative optical assessment of the reaction.

3.4.2 Heparin Immobilization

The now available amine surface capability was used to further modify the UPCL-6 surface by functionalization with the glycosaminoglycan heparin. The molecular structure of heparin is depicted in Figure 8.

The goal of heparin immobilization is to increase the affinity of the resin surface for growth factors. Therefore, heparin was covalently bound to the modified UPCL-6. This was realized by activating the carboxylic acid groups of heparin through N-hydroxysuccinimide (NHS) and 1-ethyl-3-(3-dimethylaminopropyl)-carbodiimide hydrochloride (EDC). Subsequently heparin could react with the amino-functionalized UPCL-6 forming a stable amide bond.
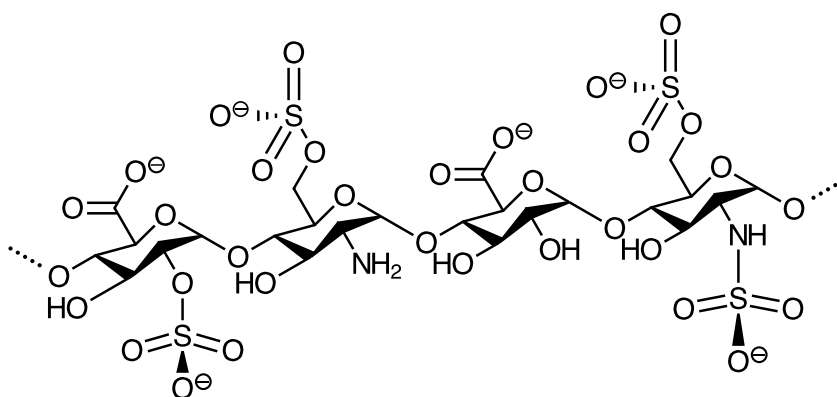
Figure 8: Molecular structure of heparin

10 mg heparin sodium salt (Sigma-Aldrich) was dissolved in 500 µL distilled water and 500 µL 1-propanol (99,9 % Sigma-Aldrich). The heparin solution (1 mg/mL) was pipetted onto each aminolyzed UPCL-6 scaffold and dried for 24 h at the room temperature. In the next step, a buffer solution of 0.1 M 2-morpholinoethanesulfanic acid (MES) (pH 5.5) dissolved in 1-propanol was prepared and EDC (12 mM) and NHS (6 mM) were added to the solution to activate the carboxyl acid groups and add the heparin onto the UPCL-6 surface. The scaffolds were incubated overnight at the room temperature and washed at least three times with distilled water to remove any unreacted material.

3.4.3 Toluidine Blue Quantification of heparin immobilization

In a next step, a quantification of the heparin immobilization was performed using a toluidine blue assay. For that 0.04 % toluidine blue (TB) solution (0,01 N HCl in 0,2 wt% NaCl) was prepared and pipetted onto the aminolyzed surface of the scaffold which had been modified with 1 mg/mL heparin. After 4 hours of incubation time, the samples were submerged in water for 5 min to remove any remaining toluidine blue solution.

Due to a detachment issue of UPCL-6 onto methacrylated coverslips, the toluidine blue quantification was only executed on scaffolds.

To calculate the amount of bound heparin on scaffolds, a standard curve was determined.

The standard curve [35] was prepared by dissolving 10 mg of heparin in 1 mL of 0.02 % NaCl solution in 0.01 N HCl and further diluted to obtain concentrations in the range expected to bind to the scaffolds.

For the standard curve following steps were used:

- Heparin (10mg/mL) was mixed with 0.04 % TB (200 µL:200 µL) and left to dissolved for 4 h at 37 °C under gentle shaking.
- The mixture was centrifuged at 3000 rcf for 10 min.
- The supernatant was removed by carefully inverting the tube.
- The precipitate was washed with 500 µl distilled water and again centrifuged at 3000 rcf for 5 min.
- The precipitate was re-dissolved with 80 % ethanol/0.1 M NaOH (4:1, v/v).
- 100 µL of the obtained solutions were used for absorbance measurement.
- The absorbance for the standard curve was determined at a wavelength of 530 nm.

For the macro-size scaffold, the steps were adjusted accordingly:

- Each scaffold was immersed in 500 µL 0,04 % TB and incubated for 4 h at 37 °C under gentle shaking.
- The scaffolds were then removed and washed with 500 µL dH$_2$O using a sonication bath to remove unbound heparin.
- The heparin-toluidine blue complex was dissolved with 80 % Ethanol/0.1 M NaOH (4:1, v/v).
- 100 µL of re-dissolved precipitate were used for absorbance measurement.
- The absorbance for the scaffold sample was determined at a wavelength of 530 nm.

3.3.4 Growth factor in vitro release Assay

To improve the bioactivity of the scaffolds, an indirect growth factor binding was attempted onto the heparin.

The used growth factor was fibroblast growth factor-2 (FGF-2PeproTech, UK) and was dissolved in sterile water to a concentration of 10 µg/mL. The macro-size scaffold was immersed for 24 h with 100 ng FGF-2 in a volume of 70 µL. The release of the growth factor (GF) was observed in a period of 21 days. The phosphate-buffered-saline (PBS, Sigma Aldrich) was refreshed on certain days and stored in the freezer at a temperature of -80 °C. For the quantification of the growth factor FGF-2 the ELISA Human FGF-basic ABTS EDK Kit (Peprotech, #0119008-M) was used.

To determine the amount of the released growth factor, a sandwich Enzyme-linked Immunosorbent Assay (ELISA) was performed. The sandwich ELISA is a sensitive method to quantify antigens between two layers of antibodies. Briefly described, the plate is first coated with a capture antibody, then the sample is added followed by an antibody functionalized with a detector. The detector then allows for a quantification of bound analyte using UV/VIS spectroscopy relating the measured intensity to a standard curve.

The ELISA for FGF-2 was performed in accordance with the protocol provided by the company. The following steps were carried out at room temperature:

- To prepare the plates for ELISA, capture antibodies of a concentration of 1 µg/mL had to be bound to the surface of the wells in the 96-well plate and incubated overnight.

- The liquid was removed, and the plates were washed for 4 times using 300 µL of wash buffer per well.

- 300 µL of block buffer were added per well and incubated for 1 hour.

- The block buffer was removed, and the plates were washed 4 times using 300 µL of wash buffer per well each time.

- Diluted standards of 100 µL were added from a range of 4000 to 0 pg/mL and triplicate per samples were added into the plate for 2 hours.

- The liquid was removed, and the plates were washed 4 times using 300 µL of wash buffer per well.

- Detection antibody of a concentration of 0.25 µg/mL was added and incubated for 2 hours.

- The detection antibody was removed, and the plates were washed 4 times using 300 µL of wash buffer.

- Avidin HRP-Conjugate was diluted in 1:2000 and 100 µL was added per well and incubate for 30 min.

- To monitor the color development, ABTS Liquid had to be added.

- The absorbance was determined at a wavelength of 405 nm with a wavelength correction of 650 nm using a plate reader.

- Color development was measured over a period for 45 min.

4 Results and Discussion

The purpose of this study was the fabrication of a bioactive macro-size scaffold that can be used for tissue engineering applications.

During the first step, a suitable 3D model for a large-size scaffold with an outer diameter of 6000 µm was designed and fabricated using the 2PP technique. Subsequently, the printing process was optimized by reducing residual THF in the resin through increased heating intervals reducing errors during the printing procedure and allowing for high-quality scaffolds to be created.

Throughout the second step, a strategy to improve the surface properties of the printed material UPCL-6 was developed. Therefore, heparin was covalently bound onto aminolyzed UPCL-6 because the glycosaminoglycan showed a high binding efficiency to several growth factors. The samples were then incubated with growth-factor FGF-2 and the release of growth factor was monitored over a period of 21 days.

4.1 Fabrication of UPCL-6 macro-size scaffold

4.1.1 Design

The designed scaffold was made by using a central porous mesh, based on interconnected repeating units resembling the diamond cubic crystal structure, and surrounded by a solid, supporting ring-shaped frame. The distance between each repeating unit was the same resulting in a uniform distribution across the scaffold. The surrounding ring frame was necessary to allow for convenient handling of the structure during the functionalization steps. The porous structure was designed to support cell growth and nutrient exchange. Throughout the experiments, the 3D-CAD models were adapted to decrease the improper stitching between adjacent FOVs. In Figure 9 the CAD design is depicted.
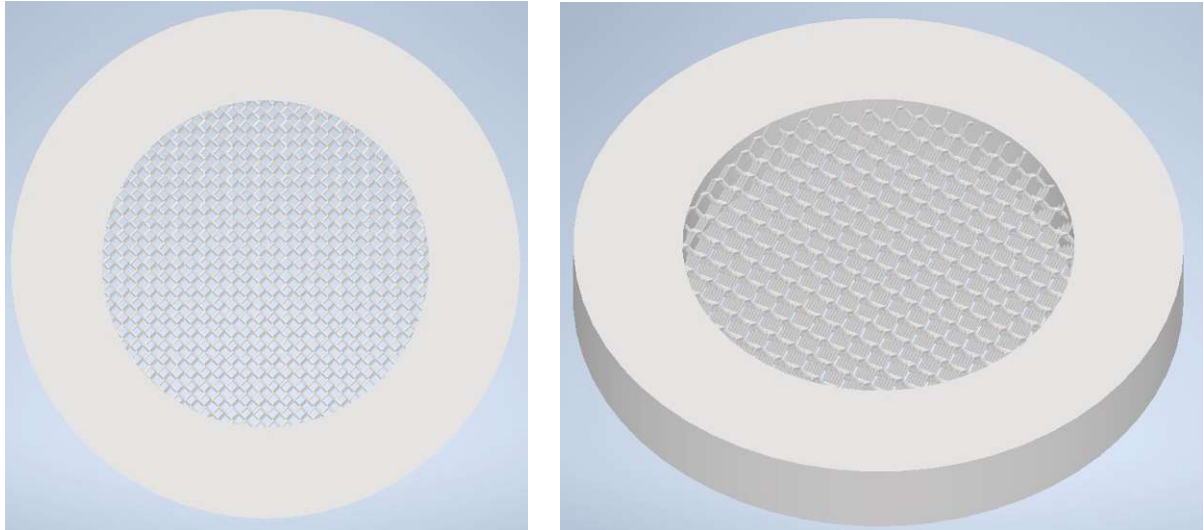
Figure 9: CAD design of the porous macro-size scaffold, left-side view from above, right-side lateral view

The first step was to find optimized printing parameters for the fabrication of a ring-shaped frame and unit cells. The outer diameter of the frame was 6000 µm and the inner diameter was 4000 µm. The height of the ring-shaped frame was 650 µm. The size of a unit cell was 300 µm that had a rod-diameter of 25 µm. In Figure 10, an optical microscope image of one of the initial structures is depicted. It is clearly visible that several rods were broken, probably during the post-processing of the sample. Most of the imperfections are visible in the middle of the scaffold. The most likely explanation is that the unit cells were not stable enough because the diameter of the chosen rods was most likely too small to obtain a robust structure.
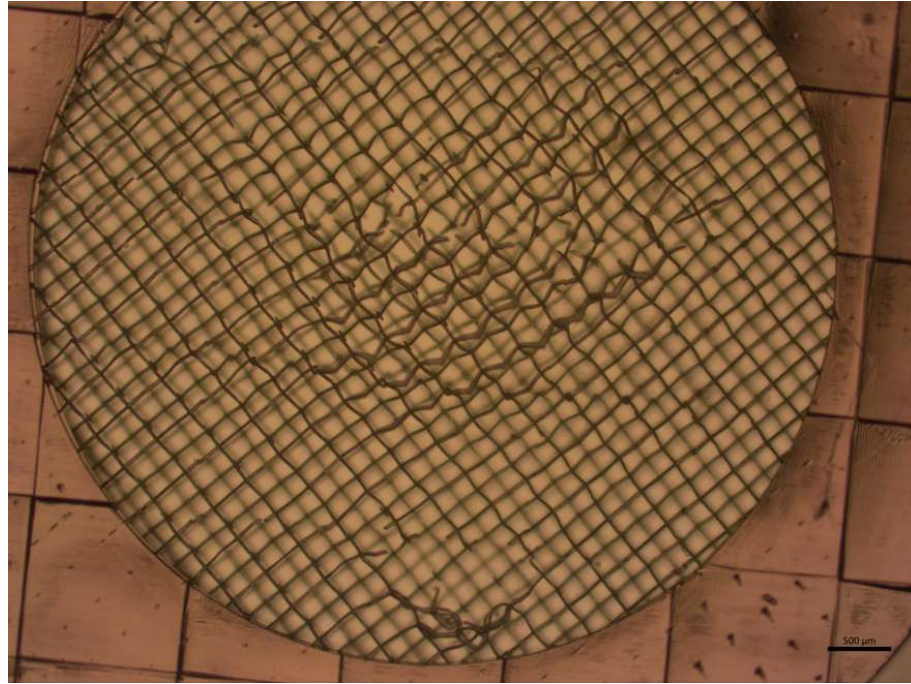
Figure 10: Optical microscopy image of a printed scaffold with a rod diameter of 25 µm

To improve the stability of the scaffold mesh, the rod diameter was increased to 35 µm and subsequently to 40 µm. A comparison between these results is presented in Figure 11. Samples printed with rod diameters of 35 µm (left side of Figure 11) still show irregularities and defects at the areas where the FOV overlap. The result on the right side of Figure 11 has a rod diameter of 40 µm and demonstrates fewer defects and shows higher stability, so 40 µm was chosen as the final rod diameter. To further decrease the defects at the stitching sites, the first layer of only the ring frame at a height of 150 µm was printed to stabilize the subsequent layers against slipping.
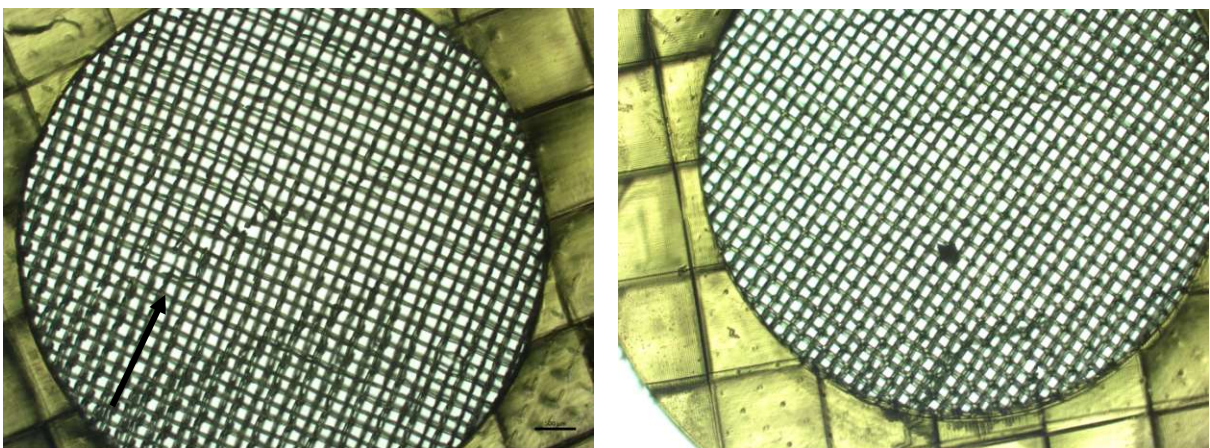
Figure 11: Optical microscopy images to compare the result of rod diameter 35 µm (left side) and 40 µm (right side)

22

The design was optimized further to achieve higher stability between the unit cells and decrease the improper stitching between adjacent FOVs. Therefore, small spheres were added at the vertices of the struts where the overlap occurs leading to the desired effect of increased stability. Luxner et. al (2007) investigated finite element modeling and described that a straightforward beam modeling in the vicinity of the verticals would suffer from deficits. Therefore, a spherical domain around each vertex is used but not by multiple overlapping beam elements.[36] A CAD design of one unit cell is depicted in Figure 12 and the final optimized design with spheres on the edges is seen in Figure 13.
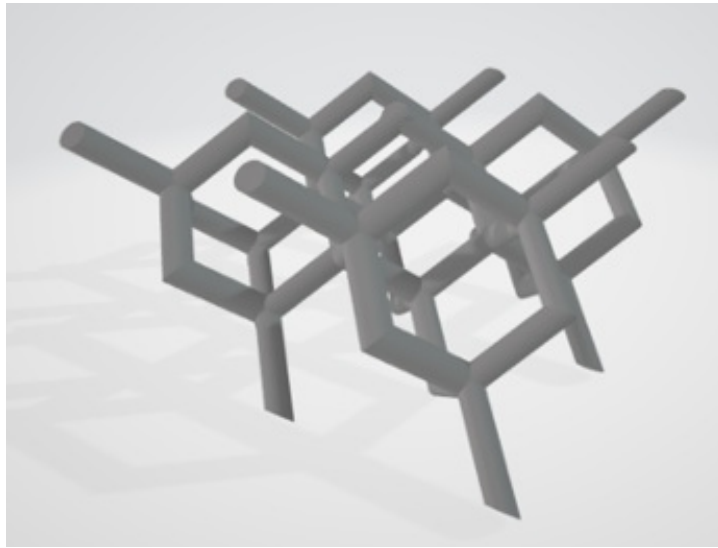
Figure 12: CAD model of four connected unit cells for macro-size scaffold
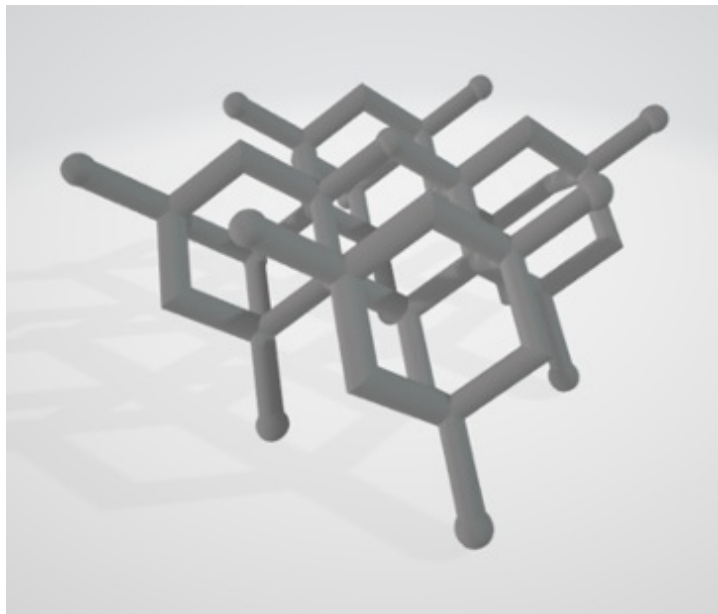
Figure 13: CAD model of four connected unit cells for macro-size scaffold with sphere on vertex

The optimal printing parameters of a suitable macro-size scaffold design can be summarized as:

- Outer diameter of macro-size scaffold: 6000 µm

- Inner diameter of macro-size scaffold: 4000 µm

- Height ring-frame: 750 µm

- Diameter of unit cell: 300 µm

- Rod diameter of unit cell: 40 µm

The XY direction still showed some improper stitching domains. A detailed analysis was performed by scanning electron microscope (SEM). An overview image of macro-size scaffolds is shown in Figure 14. The results show that it is possible to print a macro-size scaffold with a rod diameter of 40 µm. The porous structure inside the ring-frame does not show any defects on the bottom of the scaffold (right Figure 14), and on the topside (left Figure 14) one row was broken out probably during post-processing. The stitching area between unit cells is sometimes shifted in the FOV as depicted on the left image in Figure 15 compared to the right image that was acquired at a different spot of the scaffold. Therefore, the design for the unit cell was adapted with a spherical vertex as described previously to ensure an interconnection.
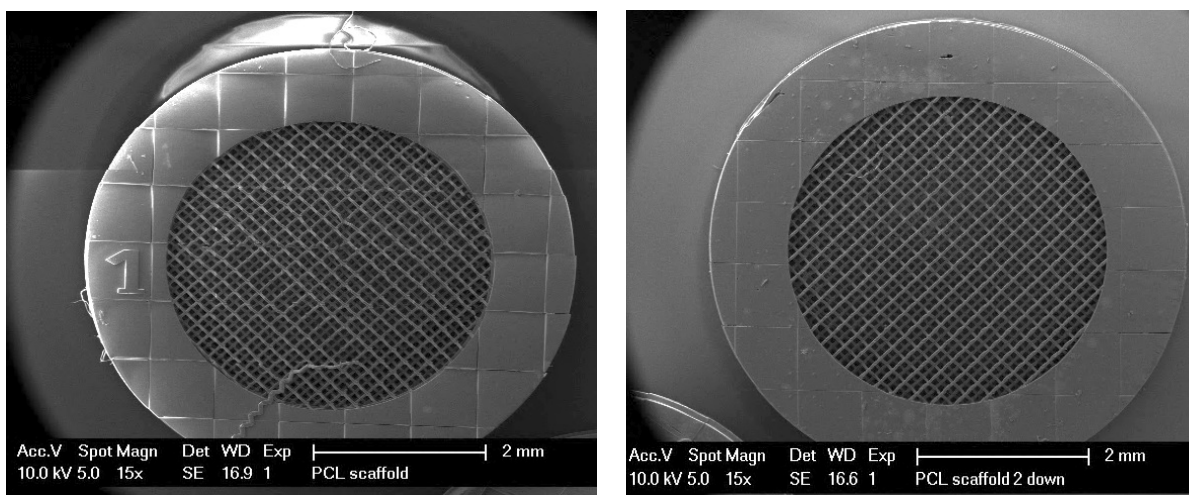
Figure 14: SEM: overview images of a printed macro-size scaffold with a 40 µm rod diameter (magnification 15x), left side an overview image of the first printed top layer, right side bottom printed layer
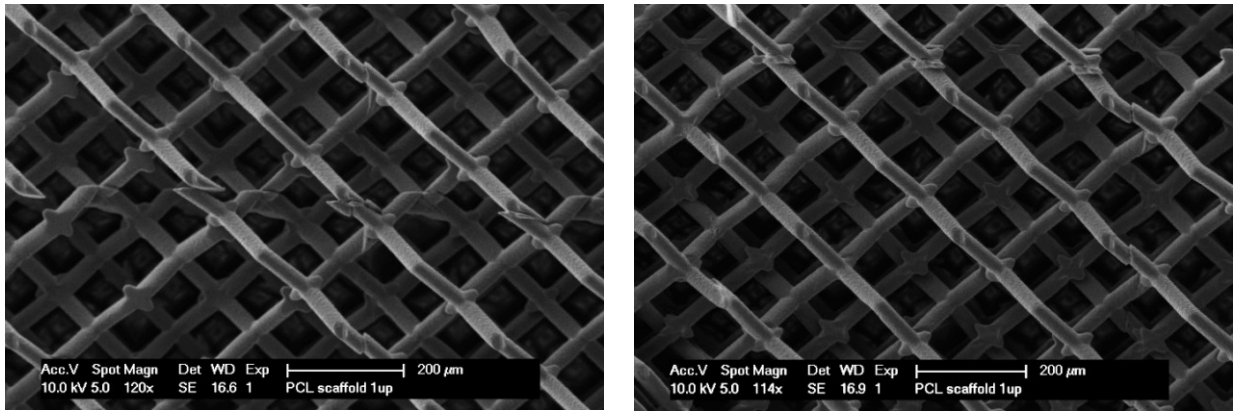
Figure 15: Detailed SEM images of printed macro-size scaffolds (40 µm rod diameter) of the stitching area (magnification 120x), left side defect in stitching area, right side proper stitching area

In the past, visible imperfections due to stitching in 2PP printed scaffolds have been reported. Gaps can be created between overlapping areas of adjacent FOVs. This is a result of the limited precision of the positioning system which is moving the printing bed in XY direction resulting in misalignments of some parts of the structure concerning each other.[10, 20] It was reported, that stitching high-porosity architectures with fine features can result in a discontinuous structure along stitching lines leading to mechanical failures of the structures.[37]. In previous research, optical imperfections were reported due to stitching between two adjacent FOVs in 2PP fabricated samples.[38] Similar problems were encountered in this work, however, they could be addressed by increasing the rod diameter and adding spherical endpoints at overlapping vertices. As a consequence, stable macro-scaffolds with good mechanical stability and high porosity were obtained.

4.1.2 UPCL-6 Material preparation

The initial preparation of the UPCL-6 material before printing proved to be also problematic. In Figure 16 improper stitching (especially visible in the top part of the ring) is very pronounced. A possible explanation is the influence of retarded THF in the resin which would change the physical properties of the resin from a solid to a more gel-like consistency in turn leading to a slight drift of the already printed parts of the structure (depicted in Figure 17).
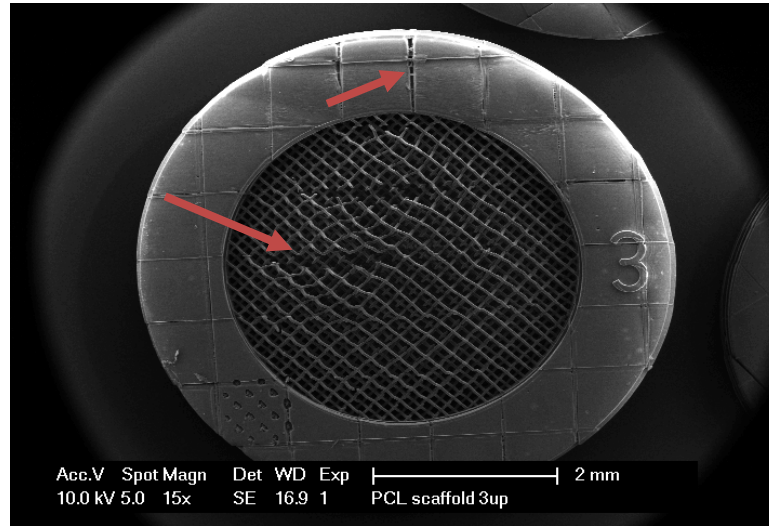
Figure 16: SEM overview image of a printed macro-size scaffold with stitching defects (rod diameter of 40 µm, magnification 15x)
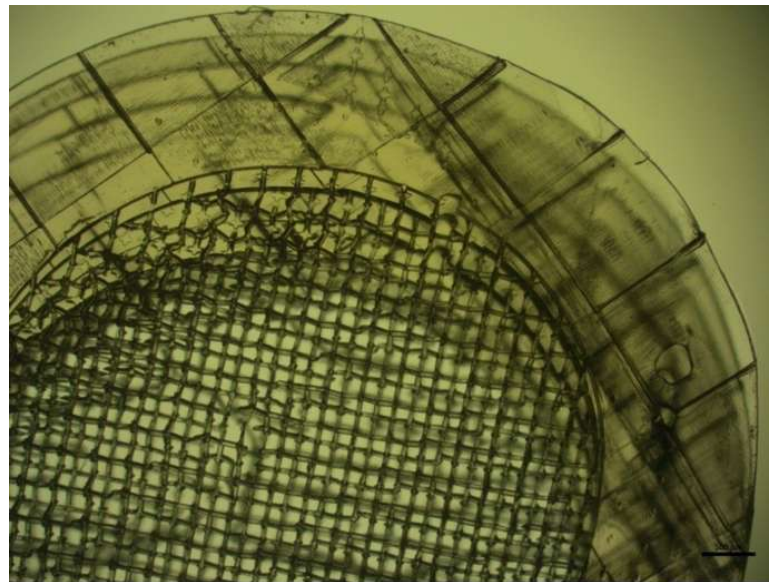
Figure 17: Optical microscopy overview image of printed macro-size scaffolds (40 µm rod diameter)

The initial method used to address this problem was to change from the bulk preparation to a layer by layer addition with the idea that thinner layers will allow for more complete removal of THF solvent.

Therefore, the method layer by layer deposition was optimized by using 250 µL of material per layer instead of 500 µl and drying in-between at 50°C for 1 hour. The resin was left overnight on the heat block at 50 °C to evaporate as much THF as possible. In Figure 18 the result is depicted and shows that the longer heating interval could address the alignment issue in the vertical direction, however, subsequent layers are still shifted. Nevertheless, the defects inside the porous mesh were not decreased and unveiled several improper stitching areas.
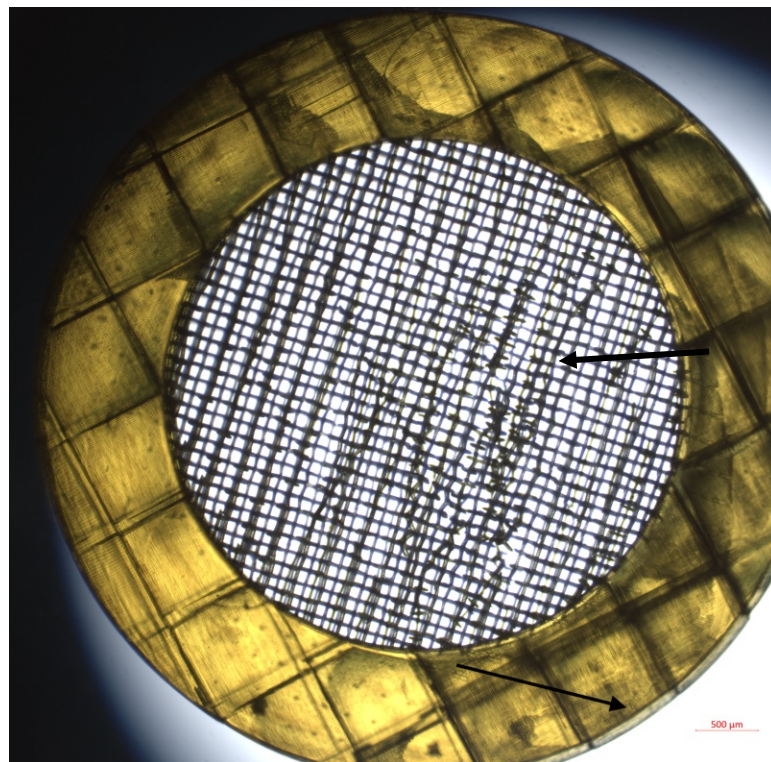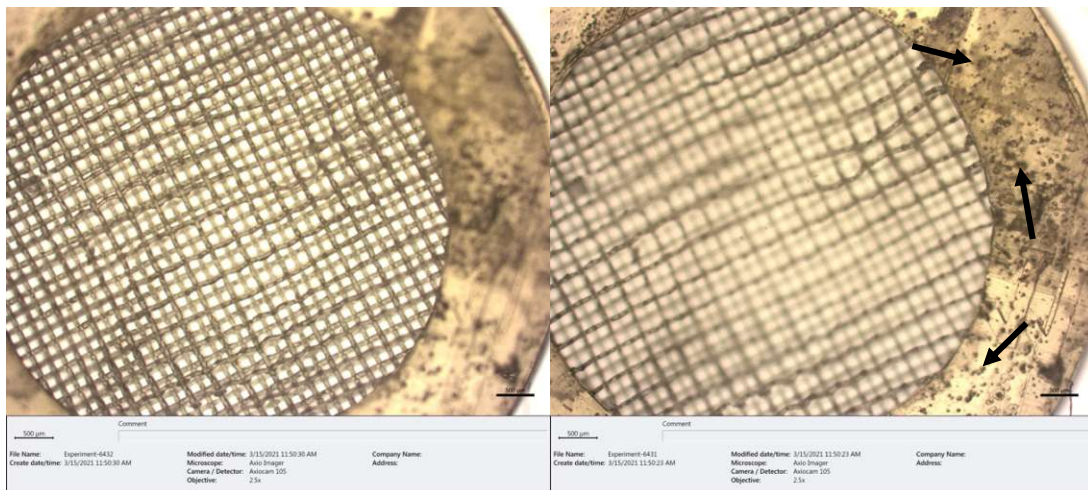

Figure 18: Optical microscopy overview image of printed macro-size scaffolds (40 µm rod diameter), material preparation by using 250 µL layers instead of 500 µL

Another approach was to modify the second method described as bulk deposition in chapter 3.3. Therefore, the UPCL-6 resin was dissolved in the stock solution and heated up to 120 °C. Different outcomes of the material preparation were tested in parallel and the distinguishing parameters are summarized in Table 2.

Table 2: Different material preparation for the resin UPCL-6

nr.	UPCL-6 weight in [g]	THF [ml]	Heated time at 120°C	Sample holder	Heated time at 70°C before printing
1	1.0817	1.44	~3 hours	Filled into sample holder and heated to 120°C for 20 min	10 min
2	0.678	0.905	~1 hour	pipet 500 µl and after 30 min the remaining material	10 min
3	1.0955	1.463	~5 hours	Filled into sample holder, UPCL-6 is very viscous	30 min
4	1.0244	1.368	~3 hours	Filled into sample holder, UPCL-6 is still very liquid	30 min

For the first preparation method the resin was dissolved in the appropriate amount of THF and PI and held at 120 °C for 3 hours. Afterward the viscous mixture was transferred to the sample holder in one go and held at 120 °C for a further 20 min and then cooled to room temperature. To obtain a transparent sample the mixture was placed at 70 °C for 10 min prior to printing. The fabricated scaffold with the first material preparation shows that the improper stitching is decreased. Some unit cells are slightly shifted (shown on the right side of Figure 19). By focusing on the frame ring (on the right side in Figure 19), a bulge in the middle of the scaffold was detected, and the material had already started to polymerize, that can be seen as dark points on the frame.

Figure 19: Optical microscopy overview image of printed macro-size scaffolds (40 µm rod diameter) with the first material preparation, left side the focus of the image is on porous mesh, right-side the focus of the image is on the frame

For the second preparation method the resin was held at 120 °C for only 1 h and was administered in two steps with 30 min in between. The resin was prepared for printing similarly to the first method. Likewise, to the sample prepared with the first method the overview image in Figure 20 also shows a bulge in the middle of the macro-size scaffold. However, the difference compared to the previously described result is that there were fewer crystals detected on the ring frame.
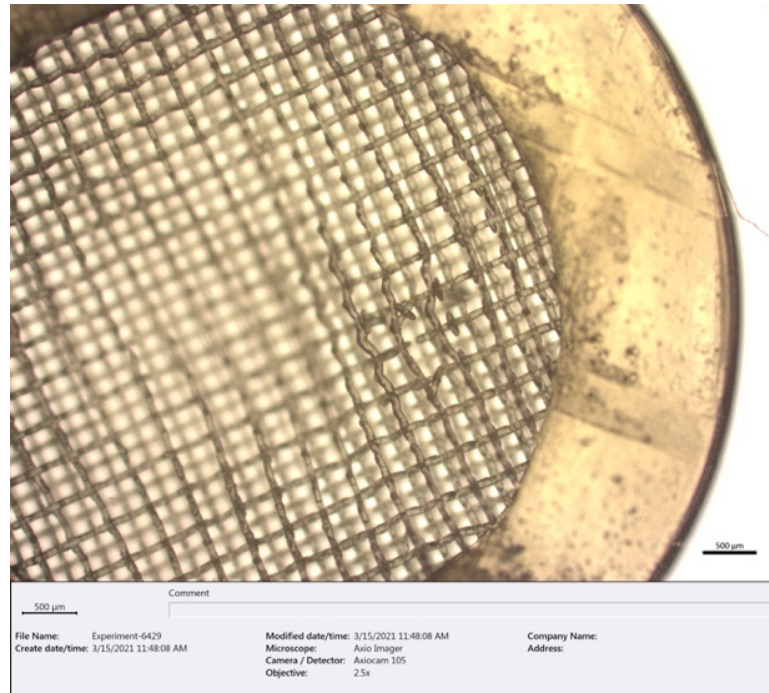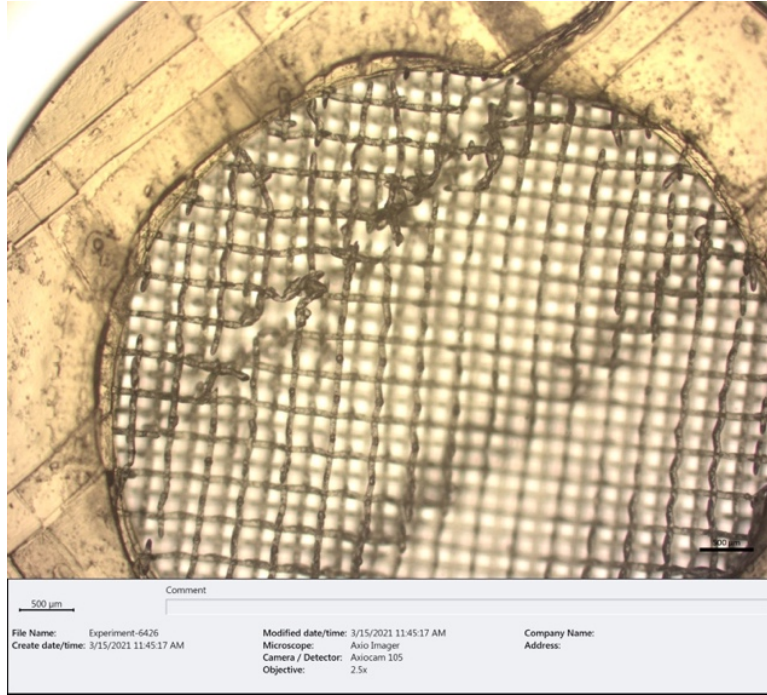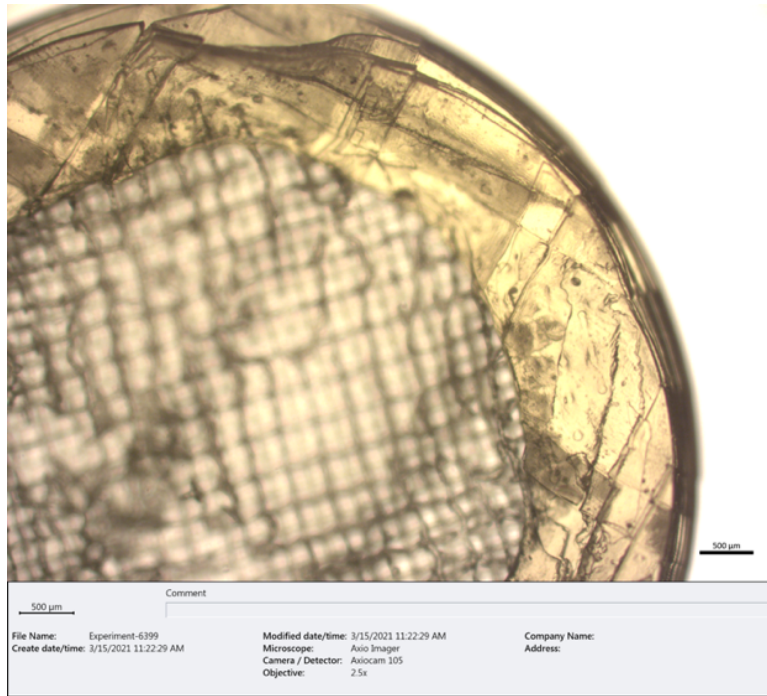

Figure 20: Optical microscopy overview image of printed macro-size scaffolds (40 µm rod diameter) with the second material preparation

The third material preparation method was similar to the first, however instead of a heating the THF, PI, resin mixture for a period of 3 h it was heated for 5 h at 120 °C and then transferred into the sample holder. Prior to printing, the resin was heated to 70 °C for 30 min, and not for 10 min as in the previous experiment. In the image of Figure 21, a whole row of improper stitching was detected, and more vertical layers were not properly positioned.

Figure 21: Optical microscopy overview image of printed macro-size scaffolds (40 µm rod diameter) with the third material preparation

The fourth material preparation was performed like the third method, however, a shorter heating time at 120 °C was used. The material appeared less viscous than in the case of the third material preparation indicating some residual THF. Nevertheless, the preparation was continued to compare the visible quality of the printed macro-size scaffold of the third and fourth material preparation.

Before the printing job was started, the material in the sample holder was heated up at 70°C for 30 min. The result is depicted in Figure 22. The focus of the image is the frame that shows that the vertical layers are shifted and that they are not in proper vertical position. Furthermore, the porous structures also show rows of improper stitching as well as the displacement of some unit cells. This proves that the quality of the printed scaffolds depends on the remaining THF in the resin.

Figure 22: Optical microscopy overview image of printed macro-size scaffolds (40 µm rod diameter) with the fourth material preparation

The influence of THF on the printing quality furthermore explains the difference in the quality of the top and the bottom layer. The increased amount of THF present decreases the viscosity of the resin causing the initially printed layers to slip during the stage movement. This in turn leads to a misalignment of the following layers causing defects and improper stitching between vertical layers.

The final selected protocol is the first way of material preparation where the resin was heated for 3 h at 120 °C, and after pipetting the resin into the sample holder, the sample was again heated up for 20 min at 120 °C. To achieve a macro-size scaffold with fewer defects, the pre-heating time of the material should not exceed 10 min because, as observed in the third way of material preparation, or the resin could be too fluid.

Arslan et al. introduced UPCL-6 as a novel material and used a concentration of 1 wt% PI M2CMK instead of the 0.5 wt% used in this work. Furthermore, the material was heated to 60°C for 2 h to evaporate the remaining THF. Their report shows no problems with this procedure, however, their structures were printed in only one FOV thus no stitching effects were visible.[25] Therefore, a comparison between both material preparation and the influence of the PI M2CMK concentration is not possible.

4.2 Biofunctionalization on macro-size scaffolds

4.2.1 Surface modification of UPCL-6 via aminolysis

The modified aminolysis protocol was first evaluated on 2D methacrylated coverslips and two different solvents were used to perform the protocol. Therefore, the influence of changing the solvent has to be investigated. As described in 3.4, the aim was to use only 1-propanol instead of an ethanol aqueous solution as solvent (1:1, v/v).

The successful aminolysis of the UPCL-6 surface was confirmed by a ninhydrin assay. The reaction of ninhydrin with free amines yields a deep purple molecule staining the samples. The red color is obtained by heating ninhydrin and indan-1,2,3-trion is formed. The negative control samples were scaffolds without any modification on the surface and therefore, not aminolyzed. Ninhydrin does not have any amines on the surface to react and is red because of the heating at 80 °C.

The results on the methacrylated coverslips are depicted in Figure 23 and did not show any difference on the performed ninhydrin assay between using ethanol/deionized water or 1-propanol. In the left petri dish, the positive aminolyzed samples are depicted, and in the right petri dish the non-aminolyzed control samples.
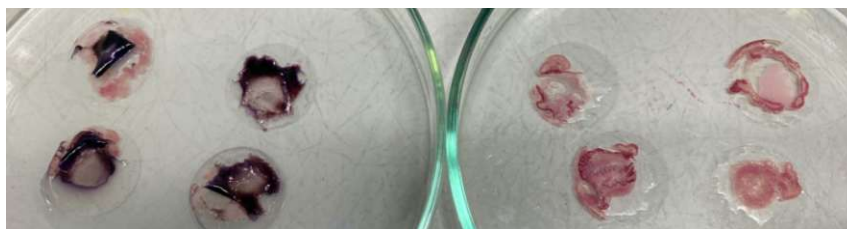
Figure 23: Ninhydrin Assay: in the left petri dish samples aminolyzed using pure 1-propanol as solvent (left) and ethanol aqueous (1:1, v/v) (right), in the right Petri dish non-aminolyzed control sample obtained with 1-propanol (left) and ethanol aqueous (right)

The modified aminolyzed protocol was performed on 3D-macroscaffolds the same way as before on 2D coverslips. As a control of the reaction, the ninhydrin assay was performed again using the same protocol.

In Figure 24, the result of ninhydrin assay on macro-size scaffolds is depicted. A clear difference between the aminolyzed sample and controlled sample without any amines is shown.

Ninhydrin reacted with free amines on the UPCL-6 surface and turned into deep blue. The control scaffold was colorless on the ring-frame and light red on the porous structure.

Figure 24: Ninhydrin assay: On the left-side aminolysed scaffold, on the right-side non-aminolyzed control scaffold

The result of the ninhydrin assay shows that the protocol of aminolysis reaction could be adapted for 3D scaffolds and amino groups were covalently introduced onto the UPCL-6 surface.

Previous research has showed that aminolysis and thus the existence of amino groups on poly- ε-caprolactone (PCL) surface decrease the water contact angle of the material and changes the surface properties from hydrophobic to hydrophilic which increase the attraction of more heparin molecules on PCL in physiological environment.[39] The functionalization of the surface will most likely lead to changes in pore size, as was reported for PCL membranes from Zhu et.al.[33] However, they could verify an aminolysis up to a depth of 50 µm. For the scaffolds fabricated in this work the high porosity of the samples makes it very likely that the complete structure is aminolyzed. However, the ninhydrin assay does not allow for a discussion of the homogeneity of coverage.

4.2.2 Heparin immobilization

After adapting the aminolysis protocol, the heparin immobilization protocol had to be modified by using, if possible, only 1-propanol as solvent instead of water.

Therefore, it was necessary to find a good ratio between 1-propanol and water to dilute heparin. Using only 1-propanol was not possible because the polarity of the solvent is too low to dissolve heparin. In Table 3 the different ratios of 1-Propanol/water are depicted. The best result to dissolve heparin proved to be 50 % 1-propanol and 50 % deionized water (1:1, v/v).

Table 3: Different ratio to soluble heparin in 1-propanol/water

1-propanol	heparin dissolved
20 %	✓
50 %	✓
70 %	✗
80 %	✗
100 %	✗

To bind heparin covalently to an aminolyzed UPCL-6 surface, the carboxylic acid groups of heparin have to be activated by using a reaction solution of NHS and EDC in MES. The control samples were also immersed with heparin but only the buffer solution was used in the subsequent step. Thereby the carboxylic acid groups could not be activated, and unbound heparin was removed during the washing steps.

For the heparin immobilization protocol, the solvent ethanol was replaced with 1-propanol. The modified protocol was first evaluated on UPCL-6 coated coverslips and compared with the original solvent ethanol. The conclusion was that the adapted steps could work but the issue was that the UPCL-6 was detached from the methacrylated glass slides.

To prove the success of the reaction, a toluidine blue assay was performed. The modified sample should change its color to pink while the control sample stays colorless. It was important to remove unreacted heparin during the washing step, especially from the control sample, otherwise the results would have been falsified.

The result of the experiment on aminolyzed UPCL-6 coated coverslips is depicted in Figure 25. Due to the detachment issue discussed above unbound heparin could not be completely removed during the washing steps thus falsifying the result. In the first row, named EDC/NHS,

heparin functionalized samples are depicted, and in the second, called EDC/NHS only MES, the control samples are shown.
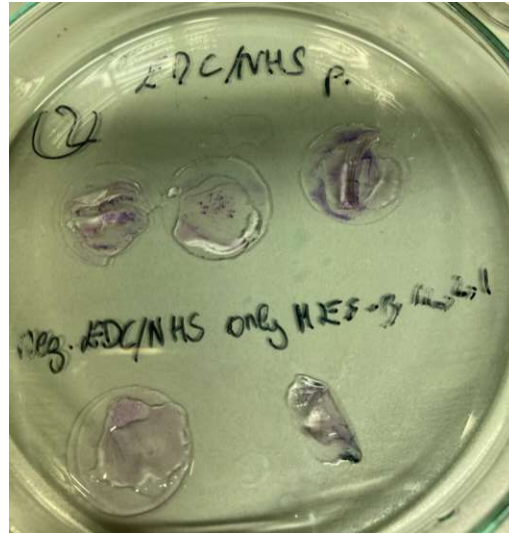

Figure 25: Toluidine blue assay on coverslips: above heparin functionalized samples, below control samples; no difference to be seen between the two groups

Due to the detachment issue of UPCL-6 on the methacrylated glasses, the modified heparin immobilization steps were repeated directly on UPCL-6 macro-size scaffolds. The toluidine blue-stained 3D-printed materials in Figure 26 show a significant difference between the positive heparin functionalized scaffold on the left side and the control scaffold on the right side.

Figure 26: Toluidine blue assay on macro-size scaffolds, left side heparin functionalized scaffold, right side control scaffold

To determine the amount of the bound heparin, a toluidine blue quantification had to be performed. Two methods of quantification were performed with different solvents because the initially chosen solvent was not able to dissolve the toluidine blue heparin complex.

For the first method of toluidine blue quantification, heparin was diluted with deionized water. The diluted heparin was mixed with 0,04 % TB solution to receive a toluidine blue complex, which, in theory, should redissolve in hexane, however this was not the case (Figure 27).

Figure 27: Toluidine blue complex did non dissolve in n-hexane

For the second method, heparin was dissolved and diluted in different concentrations with NaCl 0,2 % in HCl 0,01 N. The diluted heparin was mixed with 0,04 % TB to receive a toluidine blue complex, which was redissolved with 80 % ethanol/0.1 M NaOH instead of n-hexane. It was also possible to dissolve the toluidine blue complex on the scaffolds.

For the standard curve 14 standards were prepared (Table 4). The dissolved precipitates were determined by absorbance measurement at 530 nm and are depicted in Figure 28.

Table 4: Used amount of heparin and absorbance values for standard curve

Heparin [µg]	Absorbance measurement 1 [530 nm]	Absorbance measurement 2 [530 nm]	Absorbance measurements mean [530 nm]
200	0,871	0,966	0,9185
175	0,798	0,806	0,802
150	0,774	0,68	0,727
100	0,492	0,542	0,517
75	0,427	0,427	0,427
50	0,145	0,314	0,2295
35	0,236	0,228	0,232
25	0,181	0,188	0,1845
10	0,107	0,119	0,113
8	0,078	0,109	0,0935
6	0,085	0,089	0,087
4	0,085	0,097	0,091
1	0,083	0,061	0,072
0	0,048	0,05	0,049
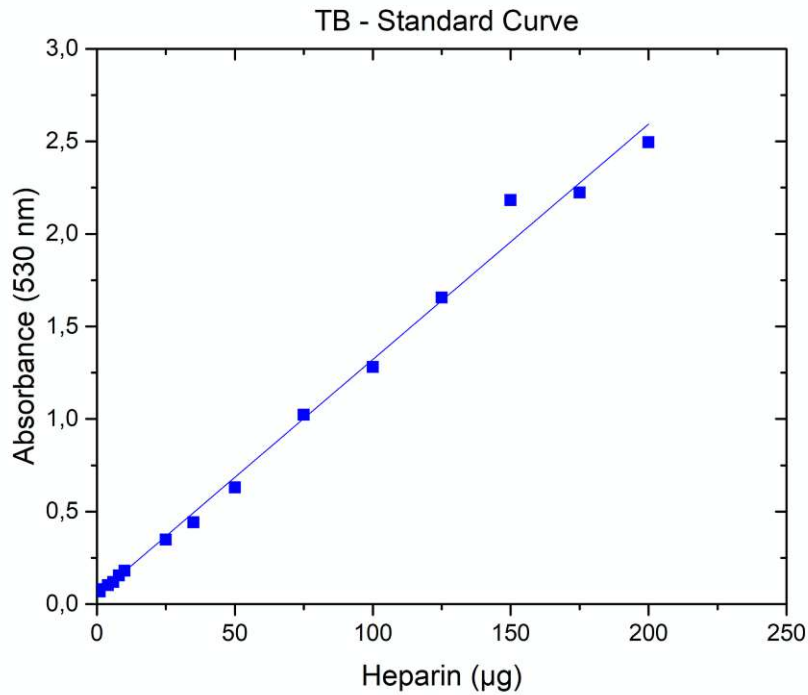
Figure 28: Standard curve for toluidine blue quantification

In figure 29 on the left side, heparin functionalized scaffolds and on the right side control scaffolds are depicted. The heparin-toluidine blue complex is still visible bound to the scaffold surface after washing with water whereas the control scaffolds are nearly colorless.

Figure 29: Toluidine Blue Quantification after the washing step to remove unbounded heparin, left-side heparin functionalized scaffolds, right-side control scaffolds without heparin

The toluidine blue complex with heparin was dissolved with an 80 % Ethanol/0.1 M NaOH solution using a sonication bath to ensure the complete removal of toluidine complex from the scaffold surface. The scaffolds after the washing step are depicted in figure 30 showing the complete removal of the blue complex.

Figure 30: scaffolds after dissolving the heparin Toluidine Blue complex (left side first performed experiment, right side second performed experiment)

The dissolved precipitates were determined by UV/VIS-spectroscopy at 530 nm and quantified with equation 3 determined from the standard curve. The resulting heparin concentrations are depicted in Table 5. The absorbance values of the macro-size scaffolds show a clear difference between the modified and control one. The calculated heparin of the positive samples is too high because each scaffold was only immersed with 100 µg of Heparin. The control samples showed that the heparin does not bind without EDC/NHS because the observed heparin concentrations was very low.

$$y = 0{,}0127 * x + 0{,}048 \tag{3}$$

Table 5: Sample absorbance and calculated amount of heparin through equation 3

scaffold	Absorbance [530 nm]	Heparin[µg]
Positive 1	2,238	172,4
Positive 2	1,131	85,3
Positive 3	2,129	163,9
Negative 1	0,123	5,9
Negative 2	0,102	4,3
Negative 3	0,058	0,8

A recently published paper shows heparin can be immobilized on PCL surface to support the biocompatibility of PCL and exhibit a significantly improved hydrophilicity. Therefore, the presence of heparin molecules improved the adsorption of positivity-charged proteins.[39]
The bound heparin on 3D aminolyzed UPCL-6 scaffolds on the surface could be proven through a toluidine blue assay. However, this method is not taken to evaluate the exact amount of heparin bound to the scaffolds.

4.2.3 Growth factor – ELISA Quantification

The final step to provide the bioactivity of the scaffold is to bind a growth factor indirectly onto the heparin. The amount of released FGF-2 over time was quantified via ELISA. As mentioned before in 3.3.4, the scaffolds were incubated with 100 ng FGF-2 in a volume of 70 µm for 24 hours.

The FGF-2 release was observed over a period of 21 days and in Table 6 the change of buffer solution is depicted.

Table 6:

Day	Day	Day
0	5	12
1	6	15
2	7	17
4	10	21

The result for the standard curve for each plate were given after 45 min. As shown in Figure 31, there was no color development as expected. Plate 1 and Plate 2 demonstrate the FGF-2 release of the biofunctionalized scaffolds and plate 3 the FGF-2 release of scaffolds without previously bound heparin.

After ELISA, the measured absorbances of standard curves are only between a range of 0.078 and 0.29. According to the company, these values have to be between 0.2 and 1.1. Therefore, the measured absorbance of the releasing of FGF-2 was not possible to interpret.

The final value of the standard curve has to be calculated by removing the wavelength correction of 650 nm from the absorbance results of 405 nm and is depicted in Figure 32.
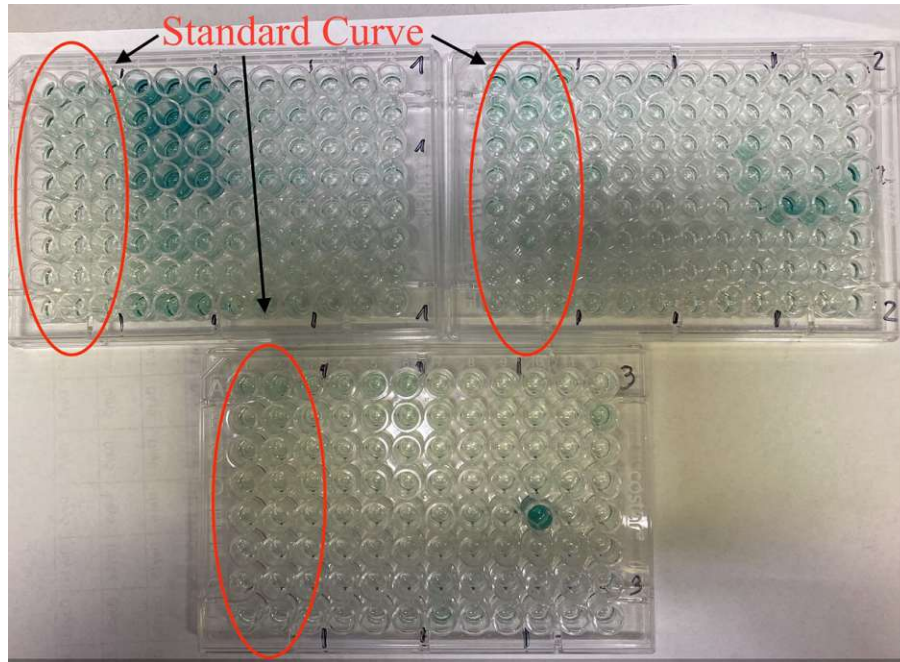
Figure 31: Color development of ELISA after 45 min, wells of standard curve are marked in red
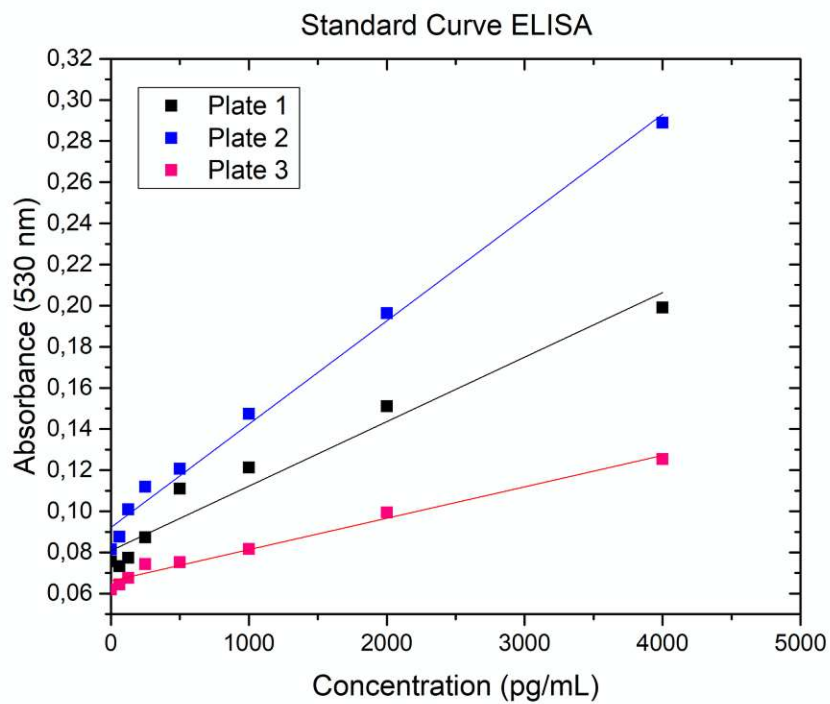
Figure 32: Standard curve of ELISA

4 heparin-functionalized scaffolds and 2 control scaffolds were incubated with 70 µL of 100 ng FGF-2.

The results of the FGF releasing of day 0 for the positive samples (plate 1) were higher than the standard curve. For day 1 the absorbance of sample 2 and sample 4 are also higher than the standard curve range. Therefore, it was not possible to interpret these results.

In the following Table 7, the calculated FGF release of each scaffold sample is depicted, and the results are also illustrated in Figure 33. The negative values are set to zero. As mention before, all samples were immersed with 100 ng FGF-2. The difference between the positive and negative samples is that the positives were biofunctionalized with heparin through EDC/NHS reaction and the negatives were not.

Table 7: Amount of FGF-2 released from the scaffolds

day	positive 1 [pg/mL]	positive 2 [pg/mL]	positive 3 [pg/mL]	positive 4 [pg/mL]	negative 1 [pg/mL]	negative 2 [pg/mL]
1	2470	5014	1903	6181	562	562
2	59	1670	648	2737	745	0
4	348	1481	103	1326	0	0
5	0	370	0	670	145	112
6	0	192	0	237	195	178
7	0	645	0	0	912	445
10	0	0	0	0	120	370
12	0	0	0	0	228	395
15	0	0	0	0	545	712
17	0	0	0	18	0	0
21	0	158	0	0	262	578
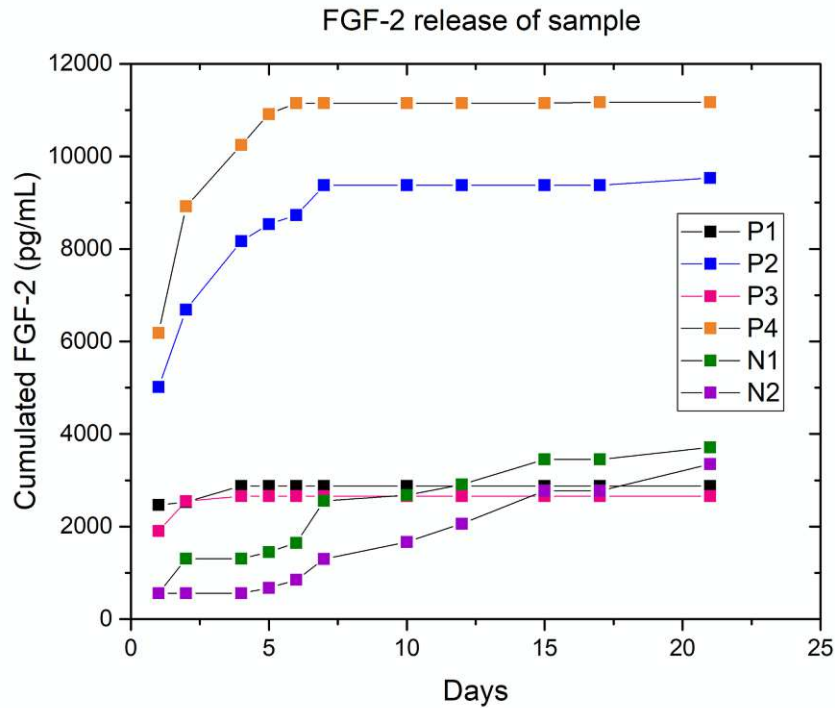
Figure 33: FGF-2 release from the scaffolds over 21 days

The results of the biofunctionalized scaffolds show that all samples release FGF-2 up until day 4, however, sample 2 and 4 continue to release some more up until day 7 and 6 respectively. The non-biofunctionalized scaffolds, on the other hand, release a constant amount of FGF-2 however, at a much lower rate.

In the previous study, it was shown that the growth factor FGF-2 can bind onto a heparin-conjugate surface of PCL. The loading efficiency was assayed by ELISA. The results showed that the heparin-conjugated sample has a higher loading efficiency than without any modification of the surface properties.[40]

5 Conclusion

In this thesis, suitable macro-size scaffolds with an outer diameter of 6000 μm and a complex porous mesh inside the ring-shaped frame were fabricated via 2PP. The modification of protocols for the biofunctionalization of UPCL-6 material allowed the scaffold to bond with bioactive properties and each step of the functionalization process could be monitored by appropriate analytical methods.

Initially, the 3D design was optimized to improve the stability of the structure. This was done by increasing the rod diameter to 40 μm as well as by terminating the rods with spheres at overlapping regions substantially decreasing stitching problems.

In combination with the improved UPCL-6 material preparation, the defects could be decreased, and suitable macro-size scaffolds were fabricated.

To optimize the bioactivity the surface was further developed to allow the attachment of growth factors. Initially, the samples were aminolyzed and subsequently heparin was attached. Both procedures were optimized by changing the solvent to better stabilize the samples in solution and thus avoid mutual sticking. The success of the aminolysis was verified with a ninhydrin assay and the heparin immobilization through toluidine blue quantification with both measurements showing a clear indication for the success of the reactions.

The controlled release experiment for FGF-2 shows that only for the initial days a release could be observed due to the low sensitivity of the employed method.

In the future, further investigation has to be done for the release amount of FGF-2 by using a more sensitive method. For osteochondral defects, a modification of the surface with growth factors related to cartilage and bone development would be of special interest. Furthermore, the influence of the modified bioactive UPCL-6 surface on stem cells should be studied.

Also, the use of a microfluidic environment in the porous macro-size scaffold, especially in the wall regions, and the elasticity and stiffness aspect during tissue maturation under in-vitro conditions, is an important aspect for the understanding of tissue growth.

List of References

1. Santin, M., *Bone tissue engineering*, in *Bone Repair Biomaterials*, J.A. Planell, et al., Editors. 2009, Woodhead Publishing. p. 378-422.

2. Mandelbaum, B.R., et al., *Articular Cartilage Lesions of the Knee.* The American Journal of Sports Medicine, 1998. **26**(6): p. 853-861.

3. Widuchowski, W., J. Widuchowski, and T. Trzaska, *Articular cartilage defects: study of 25,124 knee arthroscopies.* Knee, 2007. **14**(3): p. 177-82.

4. Zhang, B., J. Huang, and R.J. Narayan, *Gradient scaffolds for osteochondral tissue engineering and regeneration.* Journal of Materials Chemistry B, 2020. **8**(36): p. 8149-8170.

5. Nelson, A.E., *Osteoarthritis year in review 2017: clinical.* Osteoarthritis and Cartilage, 2018. **26**(3): p. 319-325.

6. King, L., L. March, and A. Anandacoomarasamy, *Obesity & osteoarthritis.* Indian Journal of Medical Research, 2013. **138**(2): p. 185-193.

7. Seo, S.S., C.W. Kim, and D.W. Jung, *Management of focal chondral lesion in the knee joint.* Knee Surg Relat Res, 2011. **23**(4): p. 185-96.

8. Ansari, S., S. Khorshidi, and A. Karkhaneh, *Engineering of gradient osteochondral tissue: From nature to lab.* Acta Biomater, 2019. **87**: p. 41-54.

9. Kang, H., Y. Zeng, and S. Varghese, *Functionally graded multilayer scaffolds for in vivo osteochondral tissue engineering.* Acta Biomater, 2018. **78**: p. 365-377.

10. Weisgrab, G., et al., *3D Printing of large-scale and highly porous biodegradable tissue engineering scaffolds from poly(trimethylene-carbonate) using two-photon-polymerization.* Biofabrication, 2020. **12**(4): p. 045036.

11. Akter, F., *Chapter 2 - Principles of Tissue Engineering.* 2016: p. 3-16.

12. Brischetto, S., P. Maggiore, and C.G. Ferro, *Special Issue on "Additive Manufacturing Technologies and Applications".* Technologies, 2017. **5**(3): p. 58.

13. Melchels, F.P., J. Feijen, and D.W. Grijpma, *A review on stereolithography and its applications in biomedical engineering.* Biomaterials, 2010. **31**(24): p. 6121-30.

14. Göppert-Mayer, M., *Über Elementarakte mit zwei Quantensprüngen.* Annalen der Physik, 1931. **401**(3): p. 273-294.

15. Andrews, D.L., *Molecular Photophysics and Spectroscopy.* Morgan & Clyapool Publishers, 2014.

16. Kaiser, W., and, and C.G.B. Garrett, *Two-Photon Exciation in Ca F 2 : Eu 2 +.* Physical review Letter, September 1961. **7**(6): p. 229-231.

17. Fourkas, J., *Multiphoton lithography, processing and fabrication of photonic structures*, in *Laser Growth and Processing of Photoniy Devices*. 2012, N.A. Vainos: Woodhead Publishing. p. 139-161.

18. Denk, W., J. Strickler, and W. Webb, *Two-photon laser scanning fluorescence microscopy.* Science, 1990. **248**(4951): p. 73-76.

19. Gruber, P., *Development of a novel wavelength-tunable high speed 2-photon lithography set up*. 2018, TU Wien

20. Steiger, W., *Investigaton of Multi-Photon Processing Parameters and Materials*, in *Institute of MAterials Science and Techniligy*. 2018, TU Wien.

21. Dehaeck, S., B. Scheid, and P. Lambert, *Adaptive stitching for meso-scale printing with two-photon lithography.* Additive Manufacturing, 2018. **21**: p. 589-597.

22. Odian, G., *Principles of Polymerization*. 4 ed. 2004: John Wiley & Sons.

23. Mandal, B., *Fundamentals of Polymerization*. 2013: World Scientific Publishing.

24. Ovsianikov, B.H.a.M.H.a.V.M.a.R.L.a.J.S.a.A., *6 - Photopolymerization-based additive manufacturing for the development of 3D porous scaffolds.* 2014: p. 149-201.

25. Aysu Arslan and Wolfgang Steiger and Patrice Roose and Hugues and Peter Gruber and Elise Zerobin and Franziska Gantner and Olivier Guillaume and Aleksandr Ovsianikov and Sandra and Peter, D., *Polymer architecture as key to unprecedented high-resolution 3D-printing performance: The case of biodegradable hexa-functional telechelic urethane-based poly-ε-caprolactone.* Materials Today, 2020.

26. O'Brien, F.J., *Biomaterials & scaffolds for tissue engineering.* Materials Today, 2011. **14**(3): p. 88-95.

27. Ovsianikov, A., A. Khademhosseini, and V. Mironov, *The Synergy of Scaffold-Based and Scaffold-Free Tissue Engineering Strategies.* Trends Biotechnol, 2018. **36**(ISSN: 0167-7799): p. 357.

28. Woodfield, T.B., et al., *Design of porous scaffolds for cartilage tissue engineering using a three-dimensional fiber-deposition technique.* Biomaterials, 2004. **25**(18): p. 4149-61.

29. Markovic, M., et al., *Hybrid Tissue Engineering Scaffolds by Combination of Three-Dimensional Printing and Cell Photoencapsulation.* Journal of Nanotechnology in Engineering and Medicine, 2015. **6**(2).

30. Kasza, K.E., et al., *The cell as a material.* Curr Opin Cell Biol, 2007. **19**(1): p. 101-7.

31. Mironov, V., et al., *Organ printing: tissue spheroids as building blocks.* Biomaterials, 2009. **30**(12): p. 2164-74.

32. Li, Z.a.P.N.a.C.K.a.T.J.a.L.S.C.a.A.A.a.H.W.a.R.A.a.V.E.a.N.S.a., *A Straightforward Synthesis and Structure–Activity Relationship of Highly Efficient Initiators for Two-Photon Polymerization.* Macromolecules, 2013. **46**(2): p. 352-361.

33. Zhu, Y., et al., *Surface modification of polycaprolactone membrane via aminolysis and biomacromolecule immobilization for promoting cytocompatibility of human endothelial cells.* Biomacromolecules, 2002. **3**(6): p. 1312-9.

34. Zhu, Y., et al., *In-depth study on aminolysis of poly(ε-caprolactone): Back to the fundamentals.* Science China Chemistry, 2012. **55**(11): p. 2419-2427.

35. Tao Liu and Yang Liu and Yuan Chen and Shihui Liu and Manfred, F.M.a.X.W.a.K.Z.a.J.W.a.Y.W.a.J.C.a., *Immobilization of heparin/poly-l-lysine nanoparticles on dopamine-coated surface to create a heparin density gradient for selective direction of platelet and vascular cells behavior.* Acta Biomaterialia, 2014. **10**(5): p. 1940-1954.

36. Luxner, M.H., J. Stampfl, and H.E. Pettermann, *Numerical simulations of 3D open cell structures – influence of structural irregularities on elasto-plasticity and deformation localization.* International Journal of Solids and Structures, 2007. **44**(9): p. 2990-3003.

37. Oakdale, J.S., et al., *Direct Laser Writing of Low-Density Interdigitated Foams for Plasma Drive Shaping.* Advanced Functional Materials, 2017. **27**(43).

38. Li, J., et al., *Two-photon polymerisation 3D printed freeform micro-optics for optical coherence tomography fibre probes.* Sci Rep, 2018. **8**(1): p. 14789.

39. Guo, J., et al., *Improved cellular bioactivity by heparin immobilization on polycarbonate film via an aminolysis modification for potential tendon repair.* Int J Biol Macromol, 2020. **142**: p. 835-845.

40. Ye, L., et al., *Heparin-Conjugated PCL Scaffolds Fabricated by Electrospinning and Loaded with Fibroblast Growth Factor 2.* J Biomater Sci Polym Ed, 2011. **22**(1-3): p. 389-406.

List of Figures

List of Tables

List of Abbreviations

2PA	Two-photon absorption
2PP	Two-Photon Polymerization
AM	Additive manufacturing
AOM	Acousto-optic-modulator
CAD	Computer-aided design
CMOS	Complementary metal oxide semiconductor
EDC	1-ethyl-3-(3-dimethylaminopropyl)-carbodiimide hydrochloride
ELISA	Enzyme-Linked Immunosorbent Assay
FGF-2	Fibroblast growth factor-2
FLD	Fused layer deposition
FOV	Field of view
GF	Growth factor
HMDS	Hexamethyldisilazane
M2CMK	4-methylcyclohexanone-based initiator
MES	2-morpholinoethanesulfanic acid
MPA	Multi-photon absorption
NHS	N-hydroxysuccinimide
PBS	Phosphate-buffered-saline
PCL	Poly- ε-caprolactone
PI	Photoinitiator
SEM	Scanning electron microscope
SLA	Stereolithography
TB	Toluidine Blue
TE	Tissue Engineering
TERM	Tissue engineering and regenerative medicine
THF	Tetrahydrofuran
TPO-L	2,4,6-trimethylbenzoyl phenylethoxyphospine oxide
UPCL-6	Hexa-acrylate end-capped urethane-based poly- ε-caprolactone